P147854.PDF [Page: 5 of 83]

Defence Research Establishment Pacific
Centre de recherches pour la défense pacifique

DEFENCE RESEARCH ESTABLISHMENT PACIFIC

CFB Esquimalt, FMO Victoria, B.C. V0S 1B0

DREP Report 93-81

NEW APPROACHES TO MAGNETIC MODELLING
I. PROLATE SPHEROIDS
II. ONE-SPIKE-AT-A-TIME FITTING

by

P.M. Holtham
Defence Research Establishment Pacific, FMO Victoria,
Victoria, B.C., V0S 1B0

and

C.E. Lucas
Barrodale Computing Services Ltd., 8-1560 Church Ave.,
Victoria, B.C., V8P 2H1

November 1993

Approved By:

Chief DREP

Research and Development Branch
Department of National Defence

Canada

Abstract

A semi-empirical model is described for parameterizing the magnetic signature of a ship or submarine in terms of a source distribution of independently magnetized prolate spheroids. The magnitudes of the components of the three-dimensional magnetization vectors for each spheroid are determined by fitting to experimentally determined field values. The equations that describe the model are shown to be valid for permanent, induced, and combined sources of magnetization. In a typical application, field values are determined from a degaussing range, and the model is used to predict signatures for mine-simulation, surveillance or ranging applications.

A description is given of the non-unique and non-realistic solution-problems that occur when least-squares methods are applied to supposedly over-determined sets of simultaneous equations which, in fact, are described by a 'rank-deficient' modelling matrix. To overcome these problems, a 'one-spike-at-a-time' technique, first developed for seismic deconvolution, was adapted for use with the magnetic model.

Examples are given of fits to simulated data, together with fits to experimentally obtained data for both non-degaussed and degaussed steel-hulled vessels.

Contents

1 INTRODUCTION 6

2 MAGNETIC MODELS AND SOLUTION PROBLEMS 7

2.1 BACKGROUND 7

2.2 SPURIOUS AND NON-UNIQUE SOLUTIONS 10

2.3 INFLUENCES ON OSCILLATORY SOLUTIONS 11

3 MATHEMATICAL ORIGINS 14

3.1 RANK-DEFICIENCY 14

3.2 SINGULAR VALUE DECOMPOSITION 15

4 CONVENTIONAL WEIGHT DETERMINATION 18

4.1 MINIMUM-LENGTH SOLUTIONS 18

4.2 SECOND DERIVATIVE CONSTRAINTS 20

4.3 COMMENT 21

5 THE PROLATE SPHEROID MODEL 21

5.1 PROLATE SPHEROID THEORY 22

5.2 INITIAL MODEL FITTING 27

6 ONE-SPIKE-AT-A-TIME FITTING 27

7 MEASURED AND MODELLED FIELDS 28

8 POSITION OPTIMIZATION 31

9 CONCLUDING REMARKS AND SUMMARY 38

A APPENDIX A 40

A.1 STANDARD LEAST SQUARES 40

A.2 RANK-DEFICIENT CASE 40

A.2.1 MINIMUM-RESIDUAL SOLUTIONS 41

A.2.2 MINIMUM-LENGTH SOLUTION 42

B FIELDS OF A MAGNETIZED PROLATE SPHEROID 44

B.1 BACKGROUND 44

B.2 PERMANENT MAGNETIZATION 47

B.2.1 LONGITUDINAL 47

B.2.2 TRANSVERSE 48

B.3 INDUCED MAGNETIZATION 49

B.3.1 LONGITUDINAL 49

B.3.2 TRANSVERSE 50

B.4 COMBINED PERMANENT AND INDUCED 50

B.5 SUMMARY AND COLLATION OF SOLUTIONS 53

B.5.1 ASYMPTOTIC LIMITS 55

C POSITION OPTIMIZATION DERIVATIVES 56

List of Figures

1 A simple single dipole approximation for the magnetization of a vessel. 8

2 Simple multi-dipole distribution 12

3 The effect of source shifts and added noise on model solutions 13

4 Singular values for the model matrices 17

5 An SVD decomposition 20

6 Possible prolate-spheroid distributions 22

7 One-spike-at-a-time fitting technique 29

8 Experimental vertical magnetic field signatures 30

9 One-spike-at-a-time fitting for non-degaussed and degaussed vessels 32

10 Measured and modelled keel-line signature comparison 33

11 Modelled vertical magnetic field signatures 34

12 Longitudinal field comparison 35

13 Athwartships field comparison 36

1 INTRODUCTION

During recent years, the magnetic modelling of ship signatures has become the focus of increasing international attention. This has, in part, arisen from the increase in modern-day computer power, and the feasibility of performing far more realistic modelling than has previously been possible. In addition, there has also been the realization that, at least in some cases, theoretical modelling can give a cost-effective alternative to traditional labour intensive techniques such as physical scale modelling. In other cases, modelling is viewed as decreasing the need to perform extensive experimental measurements which often requires expensive sensors.

In modelling studies appropriate to the magnetic signatures of naval-platforms, as in many other areas, two approaches are being developed concurrently, the so-called 'first principles' models, and the 'semi-empiric' techniques, both of which have separate roles. The first-principles approaches strive to solve Maxwell's equations explicitly, so as to predict 'a-priori' the magnetic signature of a vessel based on knowledge of its geometry and the properties of the materials used in its construction. Such techniques, which in general use finite-element methods, are computationally intensive, but when fully developed may enable the magnetic signatures of new vessels to be predicted in advance, thereby enabling signature-reduction calculations to be fed into the initial ship design. A second interest in these first-principles models is to estimate the variations that occur in the signature as a vessel transits regions of differing earth's magnetic field. If successful, this would improve the automatic setting of onboard degaussing coil currents in forward operating theatres.

Semi-empirical models, on the other hand, are designed to parameterize the measured magnetic data of a vessel, and then reproduce the signature as faithfully as possible with a minimum of computation time. Such techniques are clearly well suited to problems that require repetitive calculation of the magnetic signature, and are typically used in mine-simulation, surveillance, and magnetic ranging applications.

During the 1980's, a major incentive to develop semi-empirical models was the need to upgrade degaussing ranges to keep abreast of improvements in naval mine technology. For several countries, these upgrades required the installation of sensors to measure all three components of the magnetic field, rather than just the vertical field that had been measured historically. With the sensor count and consequent cost now tripled, any approach that would allow the elimination of sensors, with the gaps being 'filled-in' by modelling, seemed an attractive option.

While evaluating some of the earlier models for potential use in Canadian range applications, as well as for use in generating magnetic signatures for DREP's Total Mine Simulation System (TMSS), two main difficulties were encountered. The first of these was the inability of some models to accurately represent the complex structure of the magnetic field of a degaussed vessel. The second was the long-known problem of 'non-unique oscillating solutions' in which the data values appear well-fitted in a least-squares sense, but by a very unrealistic or wildly varying distribution of sources in which adjacent sources have opposite signs.

As a result of these difficulties, DREP developed a new model based on the use of magnetized 'prolate spheroids'[1] which appears equally successful for both degaussed and non-degaussed vessels. At the same time, a technique first used for seismic deconvolution[2], termed the 'one-spike-at-a-time' method, was utilized to overcome the problems of non-realistic solutions. Both of these techniques are now routinely being used for simulating the magnetic signatures of ships in mine-simulation studies.

The aim of the present article therefore, is to outline both the prolate-spheroidal modelling technique, together with the one-spike-at-a-time method. Section 2 gives a brief overview of some aspects of the earlier models together with a description of the non-uniqueness problems. Section 3 outlines the theory of the prolate spheroidal modelling technique, and Section 4 describes the method used to obtain the solution. Section 5 gives an evaluation of the model, and compares experimental results with those obtained by prediction.

2 MAGNETIC MODELS AND SOLUTION PROBLEMS

2.1 BACKGROUND

The most simplistic model for the magnetic properties of a ship or submarine is to represent the vessel by a single dipole $\vec{m}$ such as shown in Figure 1. We note that (x, y, z) are spatial co-ordinates and not related to the axes of the vessel shown here in a dive. The magnetic scalar potential at some point $\vec{r}$ is then given by the familiar expression

$$\Psi = (1/4\pi)\, \vec{m} \cdot \vec{r}/r^3 \tag{1}$$

from which the magnetic field is determined using the usual relationships $\vec{H} = -\vec{\nabla}\Psi$ and $\vec{B} = \mu\vec{H}$. In Cartesian co-ordinates, these field components can be written in matrix form as

$$\begin{pmatrix} B_x \\ B_y \\ B_z \end{pmatrix} = \frac{\mu r^{-5}}{4\pi} \begin{pmatrix} (2x^2 - y^2 - z^2) & 3xy & 3xz \\ 3xy & (2y^2 - x^2 - z^2) & 3yz \\ 3xz & 3yz & (2z^2 - x^2 - y^2) \end{pmatrix} \begin{pmatrix} m_x \\ m_y \\ m_z \end{pmatrix} \tag{2}$$

where $r = (x^2 + y^2 + z^2)^{\frac{1}{2}}$. Although shown here with the magnetic dipole aligned with the vertical axis of the vessel, the dipole can assume an arbitrary direction whose components along the three Cartesian axes are determined by fitting to experimentally obtained field values.

The above approximation to a real vessel is clearly only valid in the far-field (where r is much greater than the dimensions of the source), but is adequate and commonly used for airborne magnetic anomaly detection (MAD) applications.

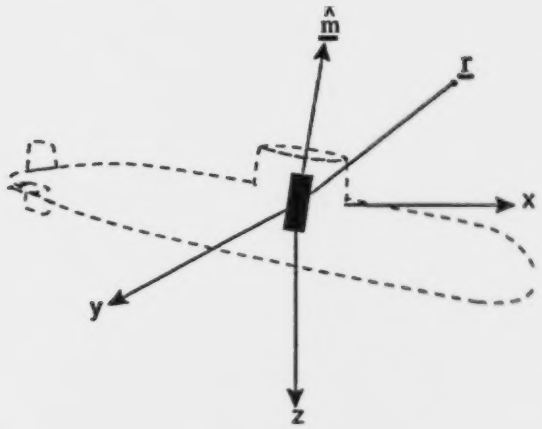

Figure 1: A simple single dipole approximation for the magnetization of a vessel.

In near-field applications, such as in mine simulation studies, the magnetic signature must be calculated at ranges from ~30 to ~200m which are similar to the dimensions of the vessel. The simple single-dipole model of (1) is totally inadequate for representing the complex structure of the field close to the hull. Several extensions of the model have therefore been developed that represent the vessel by a series of dipoles distributed throughout its interior. These include a 2-d distribution within a single plane that intersects the hull either horizontally or vertically, a full 3-d implementation where there is a uniform distribution of dipoles throughout the hull and the superstructure, and a hybrid approach, which is typically used for GRP (glass reinforced plastic or fibreglass) hulls, in which the dipoles are clustered around known sources of magnetization such as engines, pumps and weapon systems etc.

The scalar potential Ψ at some arbitrary point $\vec{r}$ can now be written as the sum over point dipoles

$$\Psi = (1/4\pi) \sum_{i=1}^{n} \vec{m}_i \cdot (\vec{r} - \vec{r}_i)/(|\vec{r} - \vec{r}_i|)^3 \qquad (3)$$

where $\vec{m}_i$ is the strength of the dipole situated on the i^{th} site. The resultant field may now be written

$$\begin{pmatrix} B_x \\ B_y \\ B_z \end{pmatrix} = \sum_{i=1}^{n} \mu r'^{-5}/4\pi \begin{pmatrix} 2x'^2 - y'^2 - z'^2 & 3x'y' & 3x'z' \\ 3x'y' & 2y'^2 - x'^2 - 'z^2 & 3y'z' \\ 3x'z' & 3y'z' & 2z'^2 - x'^2 - y'^2 \end{pmatrix} \begin{pmatrix} m_{i,x} \\ m_{i,y} \\ m_{i,z} \end{pmatrix} \qquad (4)$$

where $r' = (x'^2 + y'^2 + z'^2)^{\frac{1}{2}}$, with $x' = x - x_i$, $y' = y - y_i$ and $z' = z - z_i$. The orientations of the dipoles on different sites can well differ, and every source site can contain components along each or all of the three principal directions.

To determine the components of the dipole weights, the model is fitted to experimental field values such as those obtained during degaussing range measurements. For some such set of measurements ($\{\vec{B}_j^{meas}\}$, $j = 1...m$), m expressions similar to (4) can be written down which lead to $3m$ simultaneous equations for the $3n$ unknowns of the weights, the factor 3 having been introduced due to the vector natures[1] of both $\vec{B}_j^{meas}$ and $\vec{w}_i$. In matrix form, these equations may be written

$$\underset{\sim}{B}^{meas} = \underset{\approx}{E}\underset{\sim}{w} \tag{5}$$

where $\underset{\sim}{B}^{meas}$ and $\underset{\sim}{w}$ are the 3-component field and weight vectors expressed in linearized form as $3m \times 1$ and $3n \times 1$ column matrices respectively. $\underset{\approx}{E}$ is a $3m \times 3n$ rectangular matrix (with components $e_{i,j}$) that links the total field to the contributions produced by the individual sources, and which we term the 'modelling' matrix. Solution of (5) for $\underset{\sim}{w}$ thus gives a model source distribution that represents the measured magnetic field.

To obtain a realistic sampling of the type of complex magnetic field obtained for a degaussed steel-hulled vessel, the number of field values used for the fit is often significantly larger than the number of sources (*i.e.* $3m > 3n$), which can, in principle[2], lead to the simultaneous equations above being over-determined. When combined with the fact that $\underset{\sim}{B}^{meas}$ contains noise, (5) must in general be replaced by

$$\underset{\sim}{B}^{meas} \approx \underset{\approx}{E}\underset{\sim}{w} \tag{6}$$

and solved for $\underset{\sim}{w}$ within some least-squares framework, *i.e.*

$$\| \underset{\sim}{B}^{meas} - \underset{\approx}{E}\underset{\sim}{w} \|_2^2 = min. \tag{7}$$

As shown in Appendix A.1, the required solution for $(\underset{\sim}{w})$ satisfies the *normal* equations

$$\underset{\approx}{E}^T \underset{\sim}{B}^{meas} = \underset{\approx}{E}^T \underset{\approx}{E}\underset{\sim}{w} \tag{8}$$

where $\underset{\approx}{E}^T \underset{\approx}{E}$ is a square symmetric matrix. This expression is then usually solved, not by inverting $\underset{\approx}{E}^T \underset{\approx}{E}$ which is both computationally expensive and inexact, but by using standard numerical matrix factorization and manipulation techniques [3] [4].

[1] If only vertical magnetic fields are used for the fit, the factor 3 would be omitted from the $3m$.

[2] These equations are often, in fact, underdetermined, as discussed in Section 3

2.2 SPURIOUS AND NON-UNIQUE SOLUTIONS

Although the multiple dipole model has been used in a number of earlier works, many standard least-squares approaches used to solve (3) produce non-unique solutions. Since most of these solutions are physically non-realistic, with the dipoles often possessing abnormally large amplitudes and alternating in sign, the general applicability of the model has been limited.

Although in mathematical terms, the non-uniqueness results from the rank-deficiency of the matrix $\underset{\approx}{E}$, (see Section 3), a more intuitive origin can be found by considering the three dipoles of strengths 3, -2 and 1 in Figure 2a which represent the magnetic sources of a hypothetical one-dimensional vessel of length 80m. If we now model the vessel by 41 dipoles located at 2m intervals (*xsep*) along the ship, and fit the model to range data taken at some 20-25m depth (*drange*), then it is apparent that the dipole distribution of Figure 2b will predict almost the same field values as would those of Figure 2a. This may be seen by realizing that at the measurement distance, where $drange \gg xsep$, the two dipoles of strength 13 and -10 at location A appear like a single dipole of strength 3. Similarly those at C appear like a dipole of strength 1, and those at D′ cancel *etc.*

There are clearly a large number of spurious solutions that would be similar to, or even more complex than that of Figure 2b. Furthermore, when noise is added to the measured data and computational accuracy is introduced, it is quite possible within the least-squares framework, that one (or more) of these false solutions could be as good as or even better than the distribution of Figure 2a, and would therefore be returned by a least-squares algorithm.

Again in intuitive terms, we note that the non-uniqueness has arisen because of the closeness of the possible dipole positions with respect to the measurement distance (*i.e.* $xsep \ll drange$). There are consequently many closely spaced dipoles than can contribute almost equally to the field at a given point $\vec{r}$. The algorithm therefore has no method for differentiating between these dipoles with the result that the contribution to the field is shared between them such as in Figure 2b. Decreasing the number of dipoles would solve the non-uniqueness problem, but at the same time would severely limit the ability of the model to represent a complex magnetic field.

To demonstrate the spurious solution concept in less intuitive and more quantitative terms, we used the one-dimensional three-source linear-chain distribution of Figure 2a to generate magnetic fields similar to those obtained in a ranging environment. Three-component fields were calculated at both 10m and 20m depths on a rectangular grid from 40m ahead of the bow to 40m behind the stern, and out to 40m on either side of the vessel. Grid spacings in both the x and y directions were 5m. The source vector $\underset{\sim}{w}$ was assumed to contain only vertical polarizations, and was determined from (5) using the standard NAG Fortran library routines F01AXF and F04ANF. These routines perform a QR factorization followed by calculation of the least-squares solution. Although the resulting fits both had least-squares values of $\sim 10^{-4}\%$, the solution for the 10m-data was physically exact (Figure 2c), whereas the increased $drange/xsep$ ratio for the 20-m data caused the solution to be highly oscillatory and clearly non-realistic (Figure 2d).

This type of behaviour, namely the oscillating and non-realistic solution, which becomes more complex as $\underset{\sim}{w}$ is allowed to contain three-component sources and as noise is added to the data, typifies the difficulties that have occurred in some earlier multi-dipole models that utilize simple least-squares solutions.

2.3 INFLUENCES ON OSCILLATORY SOLUTIONS

To determine which factors have a major influence on the onset and magnitude of oscillations, we performed a series of experiments similar to those above in which source distributions were fitted to both simulated and real data using standard least-squares techniques. The findings can be summarized as follows:

covariant sources: The principle cause of oscillation was found to be the existence of covariant sources, implying that several or many adjacent sources contributed nearly equally to the field values on the measurement plane. Such covariance could be generated either by too fine a spacing of the source locations used in the fit, or by fitting to field values calculated at too large a range.

spurious data: Once the distribution of sources and the measurement distance were fixed, oscillations could be either introduced or worsened by adding noise or spurious artefacts to the data. Several common electronic artefacts were found to contribute, such as data-dropouts, incorrect gain settings, and drifts due to electronic malfunction. Common geometric artefacts also had their effect, such as the incorrect knowledge of the sensor locations, together with sensor misalignment or misorientation. For non-ferrous hulls, a discrepancy between the location of a fitting source and the true position of some discrete magnetic component also led to oscillation. Examples of the effect of a 0.25m shift in a source location, together with the effect of adding ~0.1% noise to the three-source model are shown in Figure 3 for both 10-m and 20-m fits. The oscillations have been significantly increased over those of Figure 2.

data quantity and independence: The tendency to oscillate was also affected by the quantity and independence of the data used in the fit. By using 3-component data rather than just the vertical field, and by increasing the extent of the data, either through a higher sampling frequency or by sampling for greater distances both along and perpendicular to the ship track, the stability of an otherwise marginal solution could often be improved.

These findings demonstrate that the likelihood of success for a model can be improved by utilizing as few sources as possible, and by using abundant, good quality data, taken at as close a range as possible. Unfortunately the first requirement often leads to conflict since too sparse a source distribution will give a poor fit to the complex field structures of degaussed vessels. The reduction of noise and the minimization of electronic artefacts, coupled with the ability to recognize and remove them from experimental data, will always be beneficial.

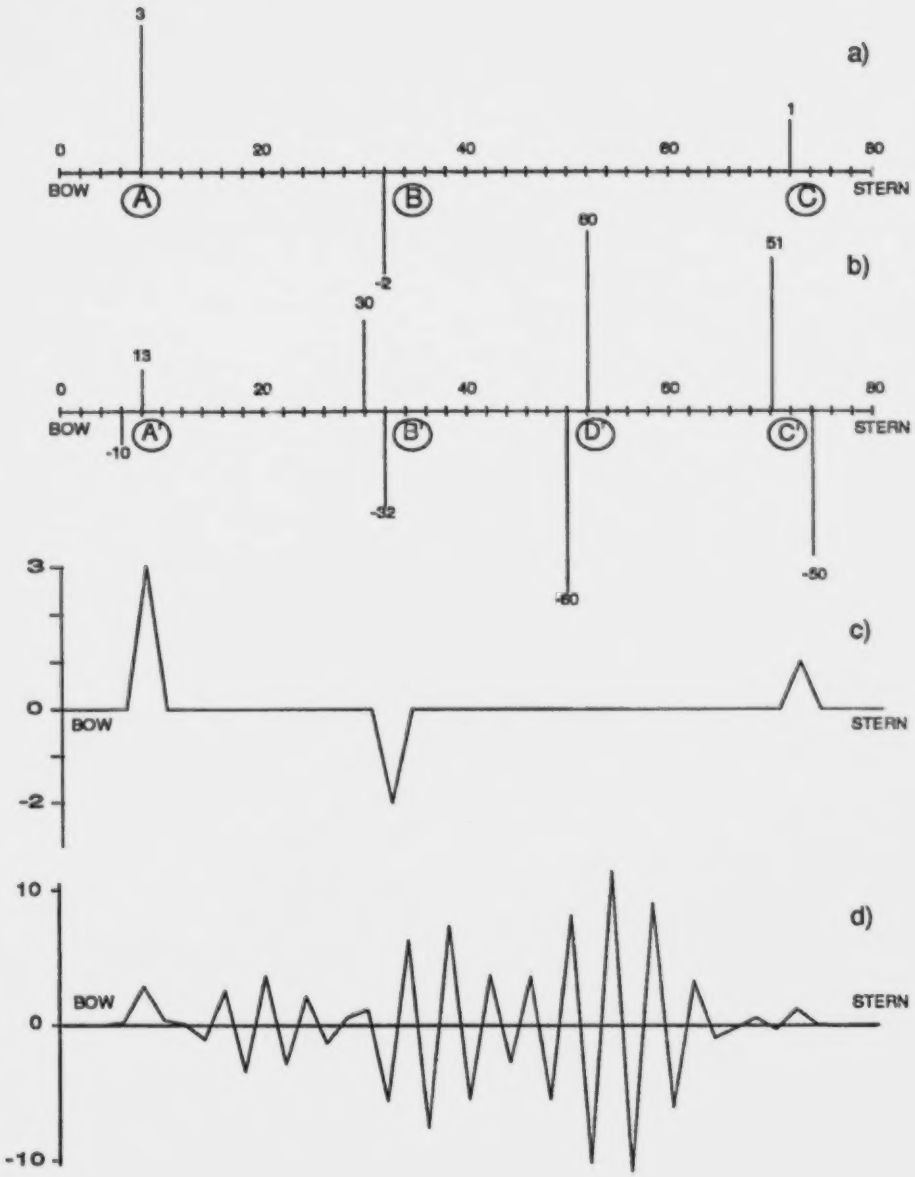

Figure 2: Simple multi-dipole distribution showing a) source weights, b) an intuitively derived non-unique fitted solution, and solutions obtained using least-squares techniques for data at measurements ranges of c) 10m, and d) 20m.

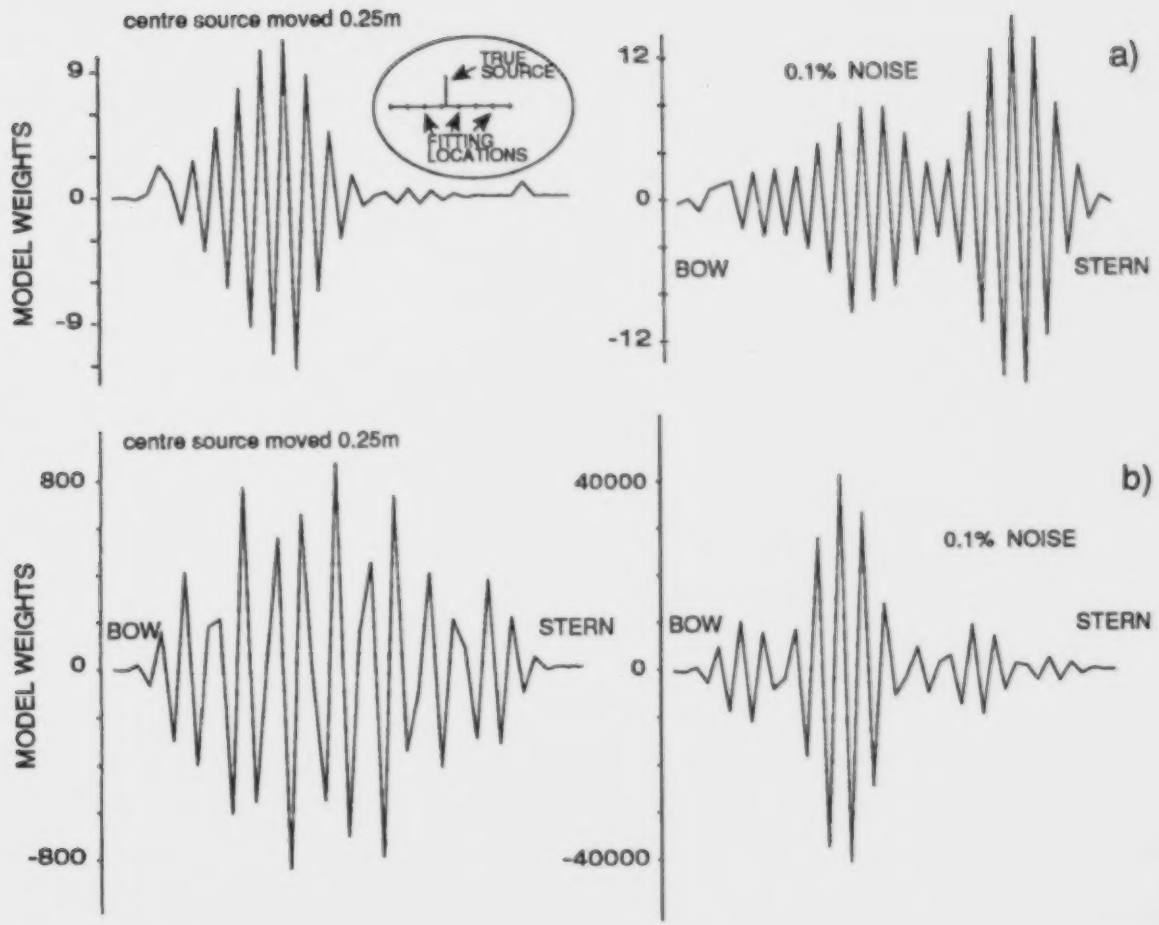

Figure 3: The effect of a 0.25-m source shift, and the addition of ~0.1% noise to the solutions of fits to the three-source model at a) 10m, and b) 20m.

3 MATHEMATICAL ORIGINS

3.1 RANK-DEFICIENCY

The results of the previous sections can be described in more rigorous terms by considering the *rank* of the model matrix $\underset{\approx}{E}$. As this concept is thoroughly discussed in standard texts[5], we simply note that the column-rank is equal to the number of linearly independent column-vectors that are found within the $3n$ column-vectors that make up the matrix. Similarly the row-rank equals the number of 3m row-vectors that are linearly independent. Since the row and column-ranks can be shown to be equal, we drop the prefixes and simply refer to the rank ρ.[3] Clearly for our situation, where $m > n$, $\rho \leq 3n$.

For the system of simultaneous equations $\underset{\sim}{B}^{meas} \approx \underset{\approx}{E}\underset{\sim}{w}$, it can be shown that if the matrix $\underset{\approx}{E}$ is of full rank (*i.e.* $\rho = 3n$), a solution exists to the normal equations (8) that is both unique and exact, apart from the usual uncertainties due to both computational and data accuracy, and provided that the equations are compatible.

When $\underset{\approx}{E}$ is not of full rank, *i.e.* with $\rho < 3n$, the solution is no longer unique as can again be seen by considering the three-spike example of Section 2.2. If two of the fitting weights w_j and w_{j+1} are assumed to be so close together that they contribute almost identically to the field values on the measurement plane, then $e_{i,j} \sim e_{i,j+1}$ for all i. The matrix relationship (6) then takes the form

$$\begin{pmatrix} B_1^{meas} \\ B_2^{meas} \\ B_3^{meas} \\ \cdot \\ \cdot \\ \cdot \\ \cdot \\ B_{3m}^{meas} \end{pmatrix} = \begin{pmatrix} e_{1,1} & \cdots & e_{1,j} & e_{1,j} & \cdots & e_{1,3n} \\ e_{2,1} & \cdots & e_{2,j} & e_{2,j} & \cdots & e_{2,3n} \\ e_{3,1} & \cdots & e_{3,j} & e_{3,j} & \cdots & e_{3,3n} \\ \cdot & \cdots & \cdot & \cdot & \cdots & \cdot \\ \cdot & \cdots & \cdot & \cdot & \cdots & \cdot \\ \cdot & \cdots & \cdot & \cdot & \cdots & \cdot \\ \cdot & \cdots & \cdot & \cdot & \cdots & \cdot \\ e_{3m,1} & \cdots & e_{3m,j} & e_{3m,j} & \cdots & e_{3m,3n} \end{pmatrix} \begin{pmatrix} w_1 \\ \cdot \\ w_j \\ w_{j+1} \\ \cdot \\ w_{3n} \end{pmatrix} \qquad (9)$$

with $\underset{\approx}{E}$ having rank $\rho = 3n - 1$. The corresponding simultaneous equations become

$$B_i^{meas} = e_{i,1}w_1 + e_{i,2}w_2 + \ldots + e_{i,j}(w_j + w_{j+1}) + \ldots + e_{i,3n}w_{3n} \qquad i = 1, 2, \ldots..3m \qquad (10)$$

which can only be solved for the sum $w_j + w_{j+1}$ and not for the two individual components. There are clearly an infinite number of possibilities for w_j and w_{j+1} that satisfy this sum, and the

[3] These definitions of rank are equivalent to the more historical definitions based on the non-vanishing minors of $\underset{\approx}{E}$ (see e.g. [6]).

solution for $\underset{\sim}{w}$ is therefore not unique. When more of the sources interact, the rank of $\underset{\approx}{E}$ decreases still further, and the number of possible solutions for $\underset{\sim}{w}$ becomes uncountably-infinite.

Consideration of the physical significance of $\underset{\approx}{E}$ indicates that each row maps the contributions of all weights to one measurement location[4], whereas a particular column maps the contribution of a single source on to all measurement locations. Given the definitions of rank based on the linear dependence of rows or columns, it is clear how rank-deficiency can be brought about by the factors discussed in Section 2.3, namely by the close spacing of source locations, by data being taken at too great a range, or by components (such as B_x and B_y) being omitted from $\underset{\sim}{B}^{meas}$.

3.2 SINGULAR VALUE DECOMPOSITION

To investigate rank-deficiency in our particular application, we used the *singular value decomposition* technique (see *e.g.* [4]) which gives the most accurate numerical determination of rank. The algorithm, which is implemented in the NAG library routine F04JGF, forms the factorization

$$\underset{\approx}{E}=\underset{\approx}{U}\underset{\approx}{\Sigma}\underset{\approx}{V}^T \tag{11}$$

where $\underset{\approx}{U}$ is a $3m \times 3m$ square matrix with $3n$ orthonormal columns, and $\underset{\approx}{V}$ is a $3n \times 3n$ orthogonal matrix. $\underset{\approx}{U}$ and $\underset{\approx}{V}$ have the properties

$$\underset{\approx}{U}^T\underset{\approx}{U}=\underset{\approx}{\mathcal{I}}^{[3n]} \quad \text{and} \quad \underset{\approx}{V}\underset{\approx}{V}^T=\underset{\approx}{V}^T\underset{\approx}{V}=\underset{\approx}{I} \tag{12}$$

and where $\underset{\approx}{I}$ is the identity-matrix and $\underset{\approx}{\mathcal{I}}^{[3n]}$ is the $3m \times 3m$ matrix containing the $3n \times 3n$ identity matrix in its upper left corner and zeroes elsewhere. Σ is the $3m \times 3n$ diagonal matrix

$$\underset{\approx}{\Sigma}= diag(\sigma_1, \sigma_2, ...\sigma_{3n}) \tag{13}$$

Formation of the products $\underset{\approx}{E}\underset{\approx}{E}^T$ and $\underset{\approx}{E}^T\underset{\approx}{E}$ yields

$$\underset{\approx}{E}\underset{\approx}{E}^T=\underset{\approx}{U}\underset{\approx}{\Sigma}\underset{\approx}{V}^T\underset{\approx}{V}\underset{\approx}{\Sigma}^T\underset{\approx}{U}^T=\underset{\approx}{U}\underset{\approx}{\Sigma}\underset{\approx}{\Sigma}^T\underset{\approx}{U}^T \tag{14}$$

and

$$\underset{\approx}{E}^T\underset{\approx}{E}=\underset{\approx}{V}\underset{\approx}{\Sigma}^T\underset{\approx}{U}^T\underset{\approx}{U}\underset{\approx}{\Sigma}\underset{\approx}{V}^T=\underset{\approx}{V}\underset{\approx}{\Sigma}^T\underset{\approx}{\Sigma}\underset{\approx}{V}^T \tag{15}$$

[4] We note that the measurements need not be coplanar.

where $\underset{\approx}{\Sigma}\underset{\approx}{\Sigma}^T$ and $\underset{\approx}{\Sigma}^T\underset{\approx}{\Sigma}$ are both diagonal matrices with elements

$$\begin{aligned}(\underset{\approx}{\Sigma}\underset{\approx}{\Sigma}^T)_{i,i} = (\underset{\approx}{\Sigma}^T\underset{\approx}{\Sigma})_{i,i} &= \sigma_i^2 \quad \textit{for } i = 1 \ldots 3n \\ (\underset{\approx}{\Sigma}\underset{\approx}{\Sigma}^T)_{i,i} &= 0 \quad \textit{for } i = 3n+1 \ldots 3m\end{aligned} \tag{16}$$

It will be noted that (15) represents the standard orthogonal transformation that diagonalizes $\underset{\approx}{E}^T\underset{\approx}{E}$ so that $\underset{\approx}{V}$ consists of the orthonormalized eigenvectors of $\underset{\approx}{E}^T\underset{\approx}{E}$. Furthermore, from (16), the quantities $\sigma_1, \sigma_2, \ldots\ldots\sigma_{3n}$, which are termed the *singular values* of $\underset{\approx}{E}$, are equal to the (non-negative) square roots of the eigenvalues of $\underset{\approx}{E}^T\underset{\approx}{E}$. Determination of the number of non-zero[5] singular values gives the rank of $\underset{\approx}{E}^T\underset{\approx}{E}$ which in turn is equal to the rank of $\underset{\approx}{E}$.

If we assume that the singular values are arranged in order of descending magnitude, and that the columns of $\underset{\approx}{U}$ and $\underset{\approx}{V}$ are rearranged accordingly, then we note from simple expansion, that when $\underset{\approx}{E}$ is rank-deficient and of rank ρ, the singular-value decomposition can be written

$$\underset{\approx}{E} = \underset{\approx_\rho}{U}\,\underset{\approx_\rho}{\Sigma}\,\underset{\approx_\rho}{V}^T \tag{17}$$

where $\underset{\approx_\rho}{U}$ and $\underset{\approx_\rho}{V}$ contain the first ρ columns of $\underset{\approx}{U}$ and $\underset{\approx}{V}$, and where $\underset{\approx_\rho}{\Sigma}$ is a square diagonal matrix of order $\rho \times \rho$. This form will be used later in Section 4.1,

Results are shown in Figure 4 for the three-spike example of Section 2.2, together with a model developed for a degaussed steel-hulled naval vessel. The three-spike field was fitted to 41 vertical polarization source sites, which leads to 41 singular values. As may be seen, the modelling matrices appropriate to 10m and 20m had respectively ~24 and ~16 singular values which differed appreciably from zero. Thus both cases were rank-deficient, leading to the spurious content in the solutions of Figures 2 and 3.[6]

For the destroyer model, where 160 three-polarization source sites were used, only some 100-120 singular values are significantly different from zero out of a total of 480. Thus, in both cases, the model matrices are highly rank-deficient, showing that despite the initial assumptions of over-determination (which were based solely on $m > n$), the simultaneous equation representations are extremely under-determined with the result that any least-squares solution will be non-unique and generally contaminated by solutions of the homogeneous equation.

[5] Due to numerical accuracy, some non-zero values may have to be set to zero if they fall below a specified tolerance.

[6] It is interesting to note that in the absence of noise the returned 10-m solution was exact (Figure 2c) even though the matrix was rank-deficient, and that oscillations occurred only when noise was added (Figure 3a). The unpredictability of apparently realistic solutions that were fortuitously returned for rank-deficient situations, was common with some earlier magnetic modelling techniques.

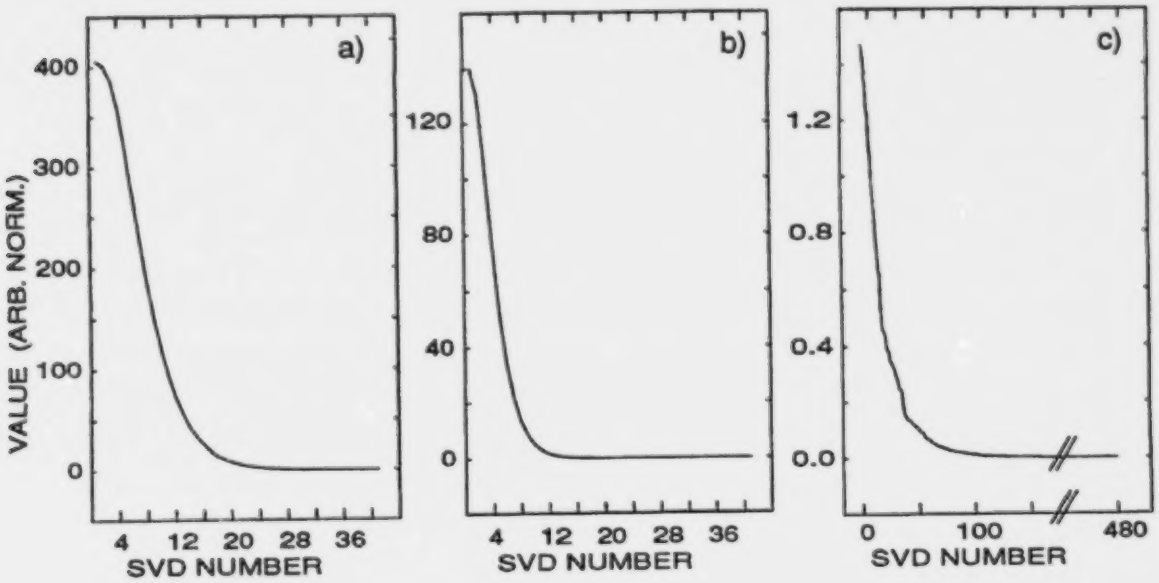

Figure 4: Singular values for the model matrices describing the three-spike-source model fitted to data at a) 10m, and b) 20m, and describing c) a degaussed steel-hulled vessel.

The origin of the difficulties experienced in many earlier studies can be seen by noting that, in practice, the smallest singular values are only close to and not identically equal to zero, as a result of noise, computational accuracy and the fact that the columns of $\underset{\approx}{E}$ are not *completely* dependent but only *approximately* dependent. Thus, in the mathematical sense, the matrix appears to be of full-rank, and a least squares algorithm (which would terminate if rank-deficency were recognized), could run to completion and yield the one solution that has the minimal residual, out of an infinite number of other vectors $\underset{\sim}{w}$ having local-minima residuals only slightly higher. Small changes in the matrix, produced by both the factors of Section 2 and computational accuracy, can change the relative magnitudes of these local minima, thereby causing an entirely different solution to be returned.

It is therefore crucial that a true rank-assessment be made before utilizing standard least-squares techniques for modelling purposes, even if the equations appear over-determined, and that other techniques be used if the rank is deficient.

4 CONVENTIONAL WEIGHT DETERMINATION

Before adopting the 'one-spike-at-a-time' technique for determining the solution for (6), we first considered two alternative methods for obtaining non-oscillatory source weights, both of which have met with success in other disciplines. These approaches included a singular value decomposition algorithm and a constrained-derivative estimation, and are briefly described below.

4.1 MINIMUM-LENGTH SOLUTIONS

In Section 2, the non-unique oscillatory solutions returned by conventional least-squares algorithms had magnitudes $\underset{\sim}{w}^T\underset{\sim}{w}$ considerably greater than would be expected for the true solution. It is therefore plausible that the most physically realistic solution could be found by locating the one particular solution, out of all solutions satisfying

$$\| \underset{\sim}{B}^{meas} - \underset{\approx}{E}\underset{\sim}{w} \|_2^2 = min. \tag{18}$$

that has minimum length

$$\| \underset{\sim}{w} \|_2^2 = min. \tag{19}$$

A particular solution to (18) can be found by using the SVD factorization $\underset{\approx}{E}=\underset{\approx}{U}\underset{\approx}{\Sigma}\underset{\approx}{V}^T$ of Section 3.2, and constructing the *pseudo-inverse* of $\underset{\approx}{E}$

$$\underset{\approx}{E}^+=\underset{\approx}{V}\underset{\approx}{\Sigma}^+\underset{\approx}{U}^T \tag{20}$$

where $\underset{\approx}{\Sigma}^+$ is the $3n \times 3m$ diagonal matrix

$$\underset{\approx}{\Sigma}^+= diag(\sigma_i^+) \tag{21}$$

with

$$\sigma_i^+ = 1/\sigma_i \text{ for } \sigma_i > 0 \text{ and } 0 \text{ for } \sigma_i = 0 \tag{22}$$

When $\underset{\approx}{E}$ is rank-deficient and of rank ρ, the pseudo-inverse can be written

$$\underset{\approx}{E}^+=\underset{\approx_\rho}{V}\underset{\approx_\rho}{\Sigma}^+\underset{\approx_\rho}{U}^T \tag{23}$$

where $\underset{\approx}{\Sigma}^{+}_{\rho}$ is a $\rho \times \rho$ square diagonal matrix, and $\underset{\approx}{U}_{\rho}$ and $\underset{\approx}{V}_{\rho}$ are the submatrices defined in Section 3.

Formation of the vector $\underset{\sim}{w}^{SVD}=\underset{\approx}{E}^{+}\underset{\sim}{B}^{meas}$ yields the *particular* solution of minimum residual to the equations $\underset{\sim}{B}^{meas}\approx\underset{\approx}{E}\underset{\sim}{w}$ as shown in Appendix A.2.

When $\underset{\approx}{E}$ is rank-deficient, the matrix $\underset{\approx}{E}$ is singular (*i.e.* $|\underset{\approx}{E}|= 0$) and any solution of the homogeneous equations $\underset{\approx}{E}\underset{\sim}{w}=\underset{\approx}{0}$ also satisfies (18) so that the general minimum-residual solutions must be written

$$\underset{\sim}{w}^{SVD} + \underset{\sim}{w}^{HOM} \tag{24}$$

of which there are an infinite number that form the set of non-unique solutions discussed earlier. By considering the lengths of these vectors, as in Appendix A.2, it can be shown that the solution with minimum length (19) is simply $\underset{\sim}{w}^{SVD}$.

In mathematical applications, where the rank of the matrix is well defined, $\underset{\sim}{w}^{SVD}$ is readily determined. For our own application, however, where only some *effective* rank ρ_{eff} can be defined, and where noise and computational accuracy become factors, a study must be made of the SVD-solution, together with the length of the vector and the sum of residuals, as the rank of the matrix is selectively reduced. An optimum solution can then be chosen based on some criterion of realism.

The results of such a study for the three-source model at 20m with approximately 0.1% noise added are shown in Figure 5a as the rank is varied between the maximum of 41 and 7, noting from Figure 4b that $\rho_{eff} \sim 16$. Calculations were made using the NAG library routine F04JGF, which performs an SVD decomposition and then sets all singular values less than some tolerance *tol* to zero before generating $\underset{\sim}{w}^{SVD}$ thus effectively decreasing the rank. Due to the large range in magnitudes, the solutions of Figure 5a are shown in scaled form.

As expected, the vector for $\rho = 41$ is identical to the standard least-squares solution, and is highly oscillatory. As the rank is reduced, the contribution of these oscillations decreases, and then at $\rho \sim 15$, the solution takes on a more realistic appearance. Unfortunately however, these more realistic solutions are still dissimilar from the true source distribution, and appear to have been heavily smoothed.

The reasons for this smoothing (which in qualitative terms arises since adjacent sources contribute nearly equally to field values on the measurement plane), can be seen from the lengths of the vectors in Figure 5b which are shown as a function of rank. For ranks below ~21, the SVD solution-length has actually become less than for the true distribution. Tests with several other simulated source distributions all showed this smoothing as the rank was forcibly decreased. This led us to conclude that the assumption of minimum-length is not well suited to applications where

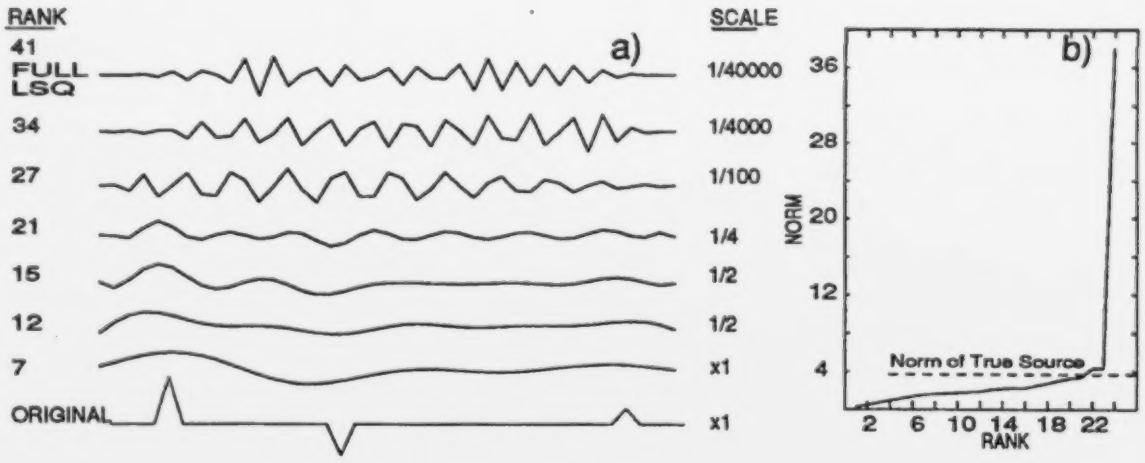

Figure 5: An SVD decomposition for the three-source model at 20m showing a) the solutions, and b) the solution lengths, as a function of forced rank.

the true source-distribution is required, and is inappropriate for the complex sources of degaussed vessels, or the discrete sources of GRP-hulled ships.

4.2 SECOND DERIVATIVE CONSTRAINTS

Recent developments in linear programming[7] have led to techniques for solving least squares problems subject to constraints on the derivatives of the weight function $\underset{\sim}{w}$. As the oscillating solutions obtained for models described by rank-deficient matrices generally have extremely large second-derivatives, it seemed appropriate to attempt to use these new techniques to minimize the residuals whilst simultaneously minimizing $\partial^2 \underset{\sim}{w} / \partial xsep^2$, $\partial^2 \underset{\sim}{w} / \partial ysep^2$, and $\partial^2 \underset{\sim}{w} / \partial zsep^2$.

If the second derivatives are written in terms of a difference equation, the problem can be formulated to minimize

$$\| \underset{\sim}{B}^{meas} - \underset{\approx}{E} \underset{\sim}{w} \|_2^2 = min. \tag{25}$$

subject to

$$(\vec{m}_{i+xsep} - 2\vec{m}_i + \vec{m}_{i-xsep})/(xsep)^2 \quad < \quad \epsilon \tag{26}$$

$$(\vec{m}_{i+ysep} - 2\vec{m}_i + \vec{m}_{i-ysep})/(ysep)^2 \quad < \quad \epsilon \tag{27}$$

and

$$(\vec{m}_{i+zsep} - 2\vec{m}_i + \vec{m}_{i-zsep})/(zsep)^2 \quad < \quad \epsilon \tag{28}$$

where ϵ is some specified tolerance, and where the notation implies that all three sites are nearest collinear neighbours along the x, y or z-direction. Since the $\vec{m}$ are vector quantities, one notes these constraints must hold for all three components, and that the constraints must be satisfied at all sites i.

A series of experiments again with both real and simulated data, however, indicated that whereas the second-derivatives were indeed reduced, the algorithm generally forced the derivative to be equal to and not less than ϵ, so that the constraint (28) was essentially treated as an identity rather than as an upper bound. The resultant solutions were not physically appealing with the result that we did not pursue the technique further.

4.3 COMMENT

In addition to the above magnetic dipole studies, similar tests were undertaken using a magnetic monopole representation, together with an analogous electric monopole representation of simulated electric fields. In each case the results were similar, with no solution being found for the oscillatory problem using least-squares techniques, and with both the minimum-length and minimum second-derivative approaches yielding unappealing solutions. We therefore chose to develop a model using a completely different set of source functions, together with a significantly different technique for determining the solution.

5 THE PROLATE SPHEROID MODEL

Section 2.3 outlined the conflicting requirements that exist when choosing the number of sources required to model a particular application. Too fine a distribution decreased the rank of the modelling matrix, thereby increasing the oscillatory nature of the solution, whereas too sparse a distribution led to a lack of detail and a decreased accuracy when modelling the complex magnetic sources of some degaussed vessels.

To overcome these problems, we extended the technique of prolate spheroidal modelling [1], in which the magnetization of the vessel is represented by a number of prolate spheroids distributed throughout the vessel. As fewer sources are now required to fill up a given volume than with

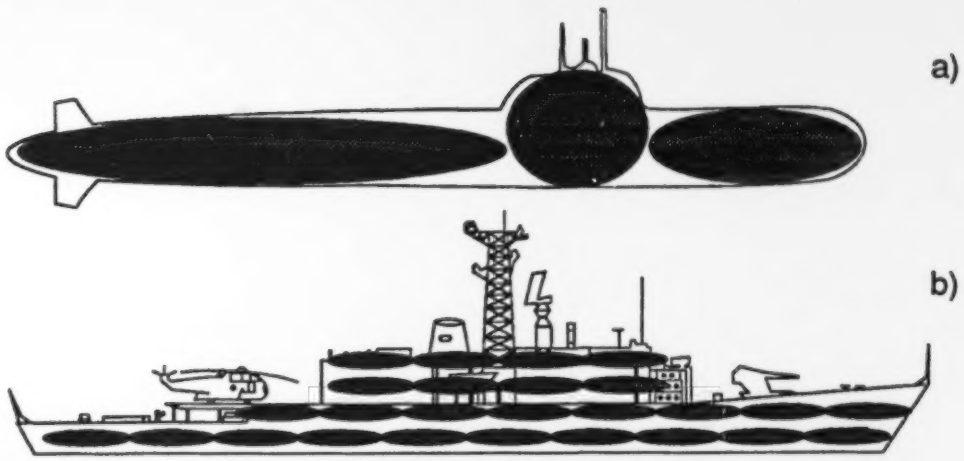

Figure 6: Possible prolate-spheroid distributions used for a) a simplistic submarine model, and b) a realistic destroyer model.

a corresponding dipole model, the model matrix is likely to be of higher rank. In addition, the representation in terms of *bulk* magnetized sources seemed more physically appealing than a representation in terms of a summation of δ-function magnetizations.

Figure 6 shows two possible spheroid distributions for a steel-hulled vessel, including a simplistic three-source model for a submarine, and then a more general model for a destroyer that uses a series of spheroids which conform to the shape of the hull. For a GRP-hulled platform such as in a mine-hunter or mine-sweeper, the spheroids can be strategically placed so as to simulate the major magnetic components. Depending on the application and modelling requirements, the spheroids can be mutually exclusive, overlapped or nested.

Whichever form of spheroid representation is used, the orientations, sizes, and magnetic contributions of the different spheroids can differ from site to site, and each site can be polarized in each (or all) of the principal directions. There are therefore an overwhelming number of possible spheroid configurations, and for simplicity in our own application, we will assume non-nested, equal sized and longitudinally oriented spheroids.

5.1 PROLATE SPHEROID THEORY

We will briefly overview the theory as the prolate-spheroid technique is comparatively new, as several equations of the reference above appear to have suffered in translation, and since the

present report extends the treatment to permanent magnetization, induced magnetization, and combinations of both. Much of the mathematical derivation will be left until Appendix B.

In the absence of any electric currents, the characteristics of the magnetic field can be described by the dc limit of two of Maxwell's equations:

$$\vec{\nabla} \times \vec{H} = 0 \quad \text{and} \quad \vec{\nabla} \cdot \vec{B} = 0 \tag{29}$$

where $\vec{H}$ and $\vec{B}$ take on their usual significance. If the medium is homogeneous and isotropic, then $\vec{B} = \mu\vec{H}$ where μ is the permeability. Under these conditions, $\vec{H}$ can be written as the gradient of a magnetic scalar potential Ψ,

$$\vec{H} = -\vec{\nabla}\Psi, \tag{30}$$

which satisfies Laplace's equation

$$\nabla^2\Psi = 0 \tag{31}$$

The solution for Ψ must satisfy the standard electromagnetic boundary conditions for $\vec{B}$ and $\vec{H}$ on the spheroid surface, and any conditions of finiteness for $\vec{H}$.

To calculate the field produced by a magnetized spheroid, we change to the prolate spheroidal coordinates (ξ, η, ϕ) (with origin at the spheroid centre)

$$\xi = \left\{ \sqrt{(x+c)^2 + y^2 + z^2} - \sqrt{(x-c)^2 + y^2 + z^2} \right\} / (2c) \tag{32}$$

$$\eta = \left\{ \sqrt{(x+c)^2 + y^2 + z^2} + \sqrt{(x-c)^2 + y^2 + z^2} \right\} / (2c) \tag{33}$$

$$\phi = \tan^{-1}(y/x) \tag{34}$$

where

$$c = \sqrt{a^2 - b^2} \tag{35}$$

is the focal length (half the inter-focal length), and where a and b are the semi-major and semi-minor axes of the spheroid respectively. The ranges of the coordinates are given by

$$1 \le \eta \le \infty, \quad -1 \le \xi \le 1, \quad \text{and} \quad 0 \le \phi < 2\pi \tag{36}$$

As shown in Appendix B, the surface of any particular spheroid can be specified by the parameters (c, η_0) where

$$a = c\eta_0 \quad \text{and} \quad b = c\sqrt{\eta_0^2 - 1} \tag{37}$$

where c is a measure of the deviation from sphericity ($c = 0$). The volume of the spheroid is given by

$$\Omega_0 = (4/3)\pi c^3 \eta_0 (\eta_0^2 - 1) \tag{38}$$

Laplace's equation can now be rewritten[7] as

$$\frac{\partial}{\partial \xi}[(1-\xi^2)\frac{\partial \Psi}{\partial \xi}] + \frac{\partial}{\partial \eta}[(\eta^2-1)\frac{\partial \Psi}{\partial \eta}] + \frac{\partial}{\partial \phi}[\frac{\eta^2 - \xi^2}{(1-\xi^2)(\eta^2-1)}\frac{\partial \Psi}{\partial \phi}] = 0 \tag{39}$$

and solved outside the spheroid by separation of variables to give

$$\Psi = \sum_n \sum_m \{a_{nm} P_n^m(\xi) + b_{nm} Q_n^m(\xi)\} [c_{nm} P_n^m(\eta) + d_{nm} Q_n^m(\eta)] \{e_m \cos m\phi + f_m \sin m\phi\} \tag{40}$$

where P_n^m and Q_n^m are the associated Legendre functions of the 1st and 2nd kind respectively, and where a,b,c,d,e and f are arbitrary coefficients.

If the magnetization is homogeneous[8] within the spheroid, the n-summation in (40) can be restricted to n=1 (see Appendix B). Further simplification can be made by imposing conditions of finiteness and symmetry. Firstly for Ψ to be finite at $\eta = \infty$, c_{nm} must be zero. Secondly, as the second associated Legendre functions are singular at ± 1, and since $\xi = 1$ and $\xi = -1$ correspond to the positive and negative x-axes respectively (outside of the spheroid), we can set $b_{nm} = 0$. Furthermore, for a magnetization parallel to the major axis, $\partial\Psi/\partial\phi$ must be zero and hence $m = 0$. Alternatively, for a magnetization transverse to the major axis, the mirror-plane symmetry demands that $m = 1$. Irrespective of the type of magnetization, Appendix B shows that the solutions can be written

$$\Psi^{out} = c\, A\, P_1^0(\xi)\, Q_1^0(\eta) \tag{41}$$

for a longitudinal magnetization,

$$\Psi^{out} = c\, B\, P_1^1(\xi) Q_1^1(\eta) \sin\phi \tag{42}$$

[7] See *eg.* Morse and Feshbach[8] and note that ξ and η are interchanged with respect to their treatise.

[8] In principle, the spheroids could contain a non-uniform magnetisation, but it is common to assume homogeneity so as to give a more tractable solution.

for a transverse y-polarized magnetization, and

$$\Psi^{out} = c\,C\,P_1^1(\xi)Q_1^1(\eta)\cos\phi \tag{43}$$

for a transverse x-magnetization.

If the three components of the spheroid source strength are written as $\vec{m} = (A, B, C)$, the magnetic field and induction can be found by calculating $-\vec{\nabla}\Psi$. As shown in Appendix B, when written in matrix form, $\underset{\sim}{H}$ and $\underset{\sim}{B}$ are given by

$$\underset{\sim}{H} = \underset{\approx}{h}\,\underset{\sim}{m} \quad and \quad \underset{\sim}{B} = \mu_0\,\underset{\approx}{h}\,\underset{\sim}{m} \tag{44}$$

where the components of $\underset{\approx}{h}$ are given by

$$h_{xx} = \frac{\eta}{\eta^2-\xi^2} - \frac{1}{2}\ell n\frac{\eta+1}{\eta-1} \tag{45}$$

$$h_{yx} = \sqrt{\frac{1-\xi^2}{\eta^2-1}}\frac{\xi}{\eta^2-\xi^2}\sin\phi \tag{46}$$

$$h_{zx} = \sqrt{\frac{1-\xi^2}{\eta^2-1}}\frac{\xi}{\eta^2-\xi^2}\cos\phi \tag{47}$$

when the magnetization is along the x or major axis of the ellipsoid.

When the magnetization is along the transverse or y-direction, we obtain

$$h_{xy} = \sqrt{\frac{1-\xi^2}{\eta^2-1}}\frac{\xi}{\eta^2-\xi^2}\,2\sin\phi \tag{48}$$

$$h_{yy} = \frac{\eta}{\eta^2-1}\left[\frac{2-\eta^2-\xi^2}{\eta^2-\xi^2}\sin^2\phi - \cos^2\phi\right] + \frac{1}{2}\ell n\frac{\eta+1}{\eta-1} \tag{49}$$

$$h_{zy} = \frac{\eta}{\eta^2-1}\frac{1-\xi^2}{\eta^2-\xi^2}\sin 2\phi \tag{50}$$

and when the magnetization is vertical we find

$$h_{xz} = \sqrt{\frac{1-\xi^2}{\eta^2-1}}\frac{\xi}{\eta^2-\xi^2}\,2\cos\phi \tag{51}$$

$$h_{yz} = \frac{\eta}{\eta^2-1}\frac{1-\xi^2}{\eta^2-\xi^2}\sin 2\phi \tag{52}$$

$$h_{zz} = \frac{\eta}{\eta^2-1}\left[\frac{2-\eta^2-\xi^2}{\eta^2-\xi^2}\cos^2\phi - \sin^2\phi\right] + \frac{1}{2}\ell n\frac{\eta+1}{\eta-1} \tag{53}$$

The transverse and vertically oriented spheroid-solutions are of course related by an interchange of y and z in the various formulae.

It is worth noting that since the equations are identical for both permanent and induced magnetizations, the model coefficients for each component separately can only be obtained by modelling the fields of ship transits on multiple geomagnetic headings, and then forming the appropriate additions and subtractions on the results.

Summation over the different spheroid sites leads to a series of expressions and simultaneous equations analogous to those of Section 2 which are then solved for the weight distribution $\underset{\sim}{w}$. In matrix form, these equations are

$$\begin{pmatrix} \begin{pmatrix} B_x^{(1)} \\ B_y^{(1)} \\ B_z^{(1)} \end{pmatrix} \\ \left(\underset{\sim}{B}^{(2)}\right) \\ \vdots \\ \left(\underset{\sim}{B}^{(\alpha)}\right) \\ \vdots \\ \left(\underset{\sim}{B}^{(m)}\right) \end{pmatrix} = \begin{pmatrix} \begin{pmatrix} h_{xx}^{(11)} & h_{xy}^{(11)} & h_{xz}^{(11)} \\ h_{yx}^{(11)} & h_{yy}^{(11)} & h_{yz}^{(11)} \\ h_{zx}^{(11)} & h_{zy}^{(11)} & h_{zz}^{(11)} \end{pmatrix} & \left(\underset{\approx}{h}^{(12)}\right) & \vdots & \left(\underset{\approx}{h}^{(1n)}\right) \\ \left(\underset{\approx}{h}^{(21)}\right) & \left(\underset{\approx}{h}^{(22)}\right) & \vdots & \left(\underset{\approx}{h}^{(2n)}\right) \\ \vdots & \vdots & \vdots & \vdots \\ \vdots & \vdots & \left(\underset{\approx}{h}^{(\alpha\beta)}\right) & \vdots \\ \vdots & \vdots & \vdots & \vdots \\ \left(\underset{\approx}{h}^{(m1)}\right) & \left(\underset{\approx}{h}^{(m2)}\right) & \vdots & \left(\underset{\approx}{h}^{(mn)}\right) \end{pmatrix} \begin{pmatrix} \begin{pmatrix} w_x^{(1)} \\ w_y^{(1)} \\ w_z^{(1)} \end{pmatrix} \\ \left(\underset{\sim}{w}^{(2)}\right) \\ \vdots \\ \left(\underset{\sim}{w}^{(\beta)}\right) \\ \vdots \\ \left(\underset{\sim}{w}^{(n)}\right) \end{pmatrix} \tag{54}$$

where the superscripted notation $\underset{\sim}{w}^{(\beta)}$ implies the three components of the weights at site β, $\underset{\sim}{B}^{(\alpha)}$

the three component field values at measurement point α, and where $\underset{\approx}{h}^{(\alpha\beta)}$ is obtained from $\underset{\approx}{h}$ by replacing $\{x, y, z\}$ by $\{x_\alpha - x_\beta, y_\alpha - y_\beta, z_\alpha - z_\beta\}$.

5.2 INITIAL MODEL FITTING

Initial fits using the prolate spheroid model indicated that although the tendency for non-realistic solutions to be returned was markedly reduced, the model matrix was still rank-deficient with the consequence that oscillatory solutions were returned by standard algorithms. We therefore decided to abandon standard least-squares and SVD approaches in favour of the *one-spike-at-a-time* method described in the following section.

6 ONE-SPIKE-AT-A-TIME FITTING

To determine the source strengths in a manner less susceptible to contamination by the non-physical non-unique solutions of the rank-deficient representation $\underset{\approx}{B}^{meas} \approx \underset{\approx}{E}\underset{\sim}{w}$, we used the so called *one-spike-at-a-time* method developed for seismic deconvolution [2]. In this technique, sources are added individually and their strengths obtained selectively, rather than all being treated simultaneously as in standard least-squares and SVD algorithms.

The technique starts by assuming an initial vector $\underset{\sim}{w}^{(0)} = \underset{\sim}{0}$ that has zero weights, with a corresponding sum of residuals given by $\mathcal{R}^0 = \| \underset{\sim}{B}^{meas} - \underset{\approx}{E}\underset{\sim}{w}^{(0)} \|_2^2 = \| \underset{\sim}{B}^{meas} \|_2^2$. The algorithm then looks at each weight in turn, and determines which particular source location would be the most effective in reducing the residual. This is done by computing the dot-products of each column of $\underset{\approx}{E}$ with $\underset{\sim}{B}^{meas}$, since, as noted in Section 3, a particular column of $\underset{\approx}{E}$ (the j^{th} say) maps the contribution of the j^{th} source onto the measurement grid. Having located this dominant contribution, a vector $\underset{\sim}{w}^{(1)}$ is constructed which contains just this one source and whose amplitude is chosen such that $\mathcal{R}^{(1)} = \| \underset{\sim}{B}^{meas} - \underset{\approx}{E}\underset{\sim}{w}^{(1)} \|_2^2 = min.$

The algorithm then searches amongst the remaining $3n-1$ columns of $\underset{\approx}{E}$ to determine a second single weight that would again be the most effective in reducing the residual. The vector $\underset{\sim}{w}^{(2)}$ is constructed which now contains two source locations, the original and the one just located. The amplitudes of the two weights are found by solving the normal equations for the system $\underset{\sim}{B}^{meas} \approx \underset{\approx}{E}^{(2)}\underset{\sim}{w}^{(2)}$, where $\underset{\approx}{E}^{(2)}$ contains just the two appropriate columns of $\underset{\approx}{E}$. A new residual $\mathcal{R}^{(2)}$ is formed where $\mathcal{R}^{(2)} < \mathcal{R}^{(1)}$

A third column is then chosen from the remaining $3n-2$ columns of $\underset{\approx}{E}$, and the amplitudes of the three sources in $\underset{\sim}{w}^{(3)}$ found by a further least-squares calculation, noting that the amplitudes of

the first two spikes may well change from their values in $\underset{\sim}{w}^{(2)}$. The process is then repeated until an adequate number of sources has been included to satisfy the problem, with previous spikes always being allowed to vary in amplitude (though not in location) whenever a new spike is added.

The algorithm is locally optimal, in that at each iteration a new source is chosen so as to achieve the largest decrease in $\mathcal{R}$. To increase this optimization, after each iteration and before locating a new column, a modified Gram-Schmidt procedure is used to orthogonalize each of the remaining columns, together with $\underset{\sim}{B}^{meas}$, to those columns already used. It is this last procedure that makes the algorithm less subject to unwanted solutions; if say three sources have nearly similar contributions on the measurement grid, then once one of these sources has been included in some $\underset{\sim}{w}^{(j)}$, the orthogonalization process ensures the other two quasi-identical sources are not included in subsequent iterations. The technique therefore returns the sparsest solution possible consistent with the data.

An example of the usage of the technique for the three-source model is shown in Figure 7, and once again the particular implementation was such that the addition of one spike implied the inclusion of one magnetization which could be an x, y, or z-polarization. As may be seen, inclusion of the initial sources leads to the population of x-magnetizations, which, since the true source is composed solely of z-magnetizations, results in a large residual error. As more spikes are introduced, however, the x-magnetizations are slowly replaced by z-polarizations, and the residual error falls significantly. At ~10 magnetizations, the solution has stabilized and there is a region of little change in either spike content or residual error. As yet more spikes are introduced, the residual error decreases insignificantly, but the source distribution begins to oscillate. Clearly the inclusion of too many sources is forcing the algorithm to utilize columns of $\underset{\approx}{E}$ that are nearly dependent on columns used previously. Up to this point of lack of stability, however, the technique is clearly returning physically realistic solutions.

The determination of the optimum number of sources for a particular model must be guided by both the residual error and the stability of the solution. In all of the present applications, the number of sources was determined by skilled observation, but in any fully automated algorithm, source cut-off would be determined by monitoring both $\mathcal{R}^{(j)}$ and $\| \underset{\sim}{w}^{(j)} \|_2^2$.

An example of the technique when used with real ship data is presented in Section 7.

7 MEASURED AND MODELLED FIELDS

To evaluate the new model and fitting techniques, we parameterized the signatures of several degaussed and non-degaussed steel-hulled vessels obtained during standard degaussing range measurements. The data consisted of three-component field values collected on each of sixteen sensor sites separated by 4.6m transverse to the ship track. Data points were recorded from one-half ship

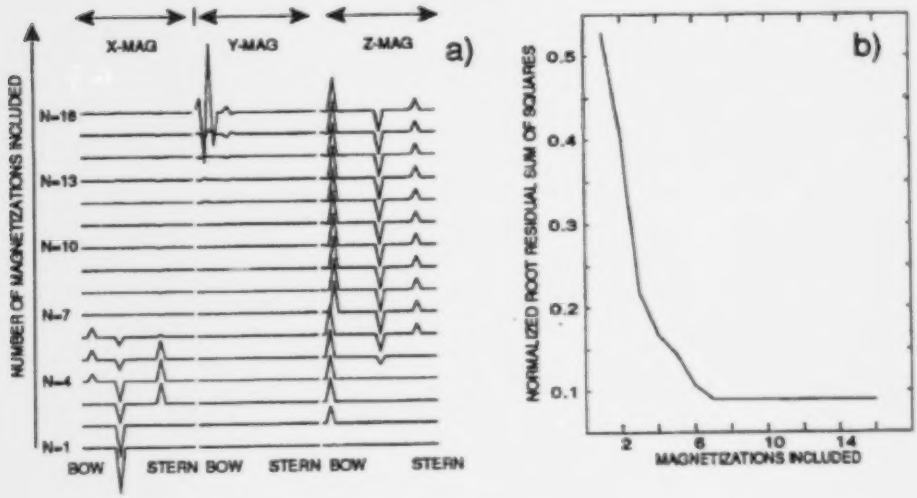

Figure 7: One-spike–at-a-time fitting technique applied to three-source model showing a) evolution of the solution, and b) the normalized square-root of the residual square error.

length ahead of the bow to one-half ship length astern. The sensors were in approximately 16m of water, and the vessels were ~100-150m in length. The sampling rate was chosen so as to obtain 256 longitudinal measurements, which for typical ship lengths and transit speeds corresponds to an ~1-1.25m spacing. There were thus 12288 data points, which for a 160 three-polarization source model leads to a model matrix $\underset{\approx}{E}$ with 5,898,240 elements. Data were sometimes subsampled by a factor 4 to reduce computational requirements, without significant loss in accuracy.

We will present the results of just two models which typify our findings, and which include both the non-degaussed and degaussed signatures shown in Figure 8. The non-degaussed signature (Figure 8a) demonstrates the familiar bell-like form arising from the vertical magnetization, together with a sub-peak towards the stern and a much smaller sub-peak towards the bow. The degaussed signature (Figure 8b), shown on a different scale, is considerably more complex, and as can be seen from the accompanying contour plot (Figure 8c) has a marked degree of asymmetry. We note that, due to the varying ship tracks, the experimental signatures are not centred laterally within the plotting grid; the model results shown below are both centred and plotted over a slightly wider athwartships range.

The results of the one-spike-at-a-time fitting process are shown in Figure 9, and again both the non-degaussed and degaussed results are on different scales. Observation of the spike-evolution, together with the residual sum of squares indicates that the non-degaussed model has converged

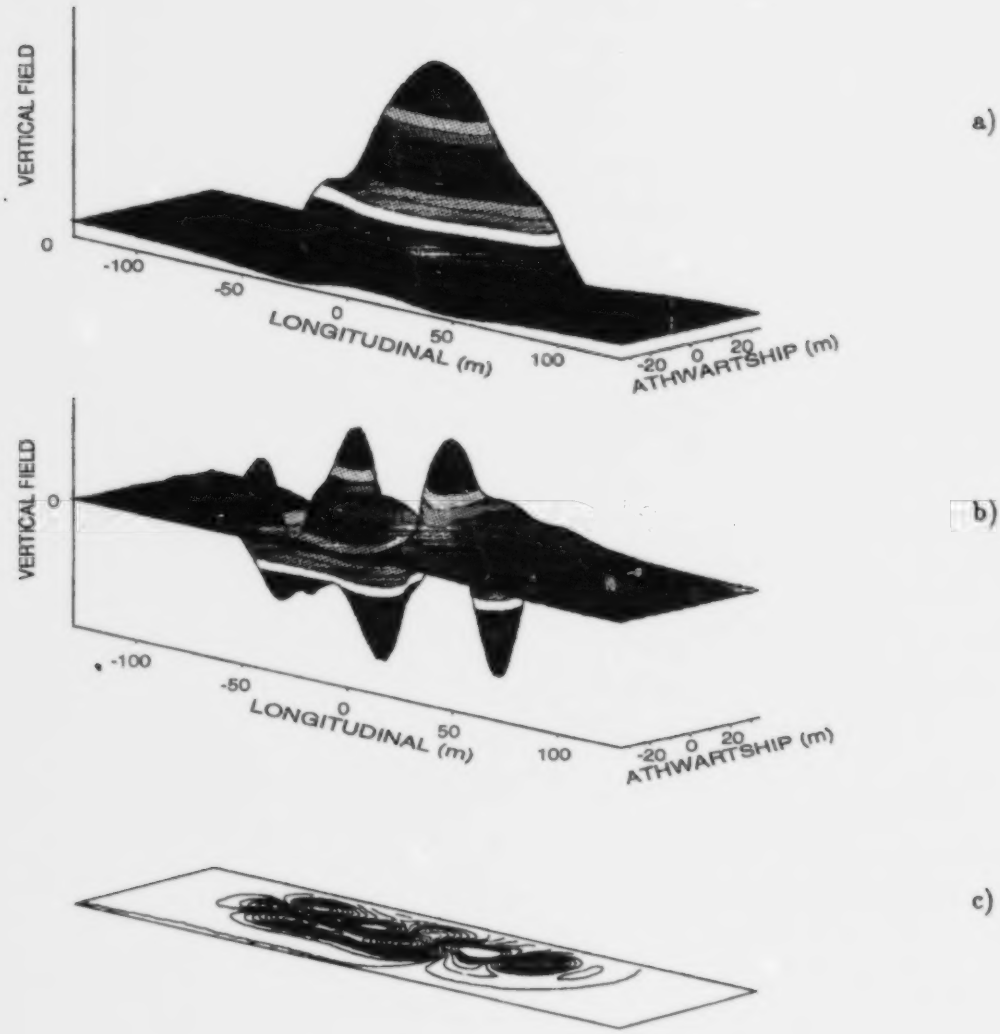

Figure 8: The vertical magnetic field signatures used during the fits for a) a non-degaussed, b) a degaussed vessel, with c) showing a contour plot of the degaussed signature.

after some 25-35 magnetic polarizations, and the degaussed model by some 35-45 polarizations. If more spikes are included, the solutions begin to oscillate, as can be seen from the 60- and 70-spike traces of Figure 9a and the 70-spike trace of Figure 9b. It is reassuring to see that the non-degaussed results have returned predominantly vertically polarized magnetizations, whereas the degaussed model confirms the degaussing coils have successfully removed the vertical magnetization, leaving a mainly longitudinally polarized residual. Such a spike-presentation might be of use to range staff during the degaussing process.[9]

A comparison of both the measured and modelled keel-line data for all three field components is shown in Figure 10, and as may be seen the agreement is good with the poorest agreement being for the degaussed athwartships field. As tests showed that shifts in vessel or sensor position by as little as 0.5m were sufficient to affect the higher frequency structure in this component, the discrepancy was not judged significant. An estimation of the root mean square error computed for all three components across the entire measurement plane is ~5-7%. We suspect this error is dominated by known uncertainties in the data, such as electronic drifts and small sensor misalignments, rather than by the modelling process itself. The present accuracy, however, has proved adequate for all of our modelling needs.

Figure 11 indicates the modelled vertical fields for both the non-degaussed and degaussed vessels, which shows good agreement with the measured values of Figure 8. The further comparisons in Figures 12 and 13 of the longitudinal and athwartships fields for the more complex degaussed signatures also shows good agreement.

Fits made to the various other ships' signatures all gave agreements qualitatively very similar to the results above.

8 POSITION OPTIMIZATION

In specifying the source distribution for a model, some decision must be made concerning the location of the individual spheroids together with their focal lengths c, and it is always of interest whether some small change would lead to an improved fit. We therefore decided to evaluate the technique proposed by Yan *et al.*[1] for optimizing the positions, although we noted that it was probably more valuable for their situation where only a few spheroids were employed. The technique is, however, much more easily applied within the one-spike-at-a-time framework, and has therefore been modified slightly from the original treatment.

After the initial fitting process, some number n_f of non-zero weights have been returned which we describe as $\underset{\sim}{w}_f$. If we define $\underset{\approx}{E}_f$ to contain just the n_f appropriate columns of $\underset{\approx}{E}$, then $\underset{\sim}{w}_f$ is

[9] Unlike Figure 7, the spike positions along the x-axes of Figure 9 are not simply related to the distance between the bow and stern due to the three-dimensional nature of the source distribution. A 3-d plot of the weights shows that the magnetisation is distributed throughout the vessel, and not close to the bow as might be thought from Figure 9.

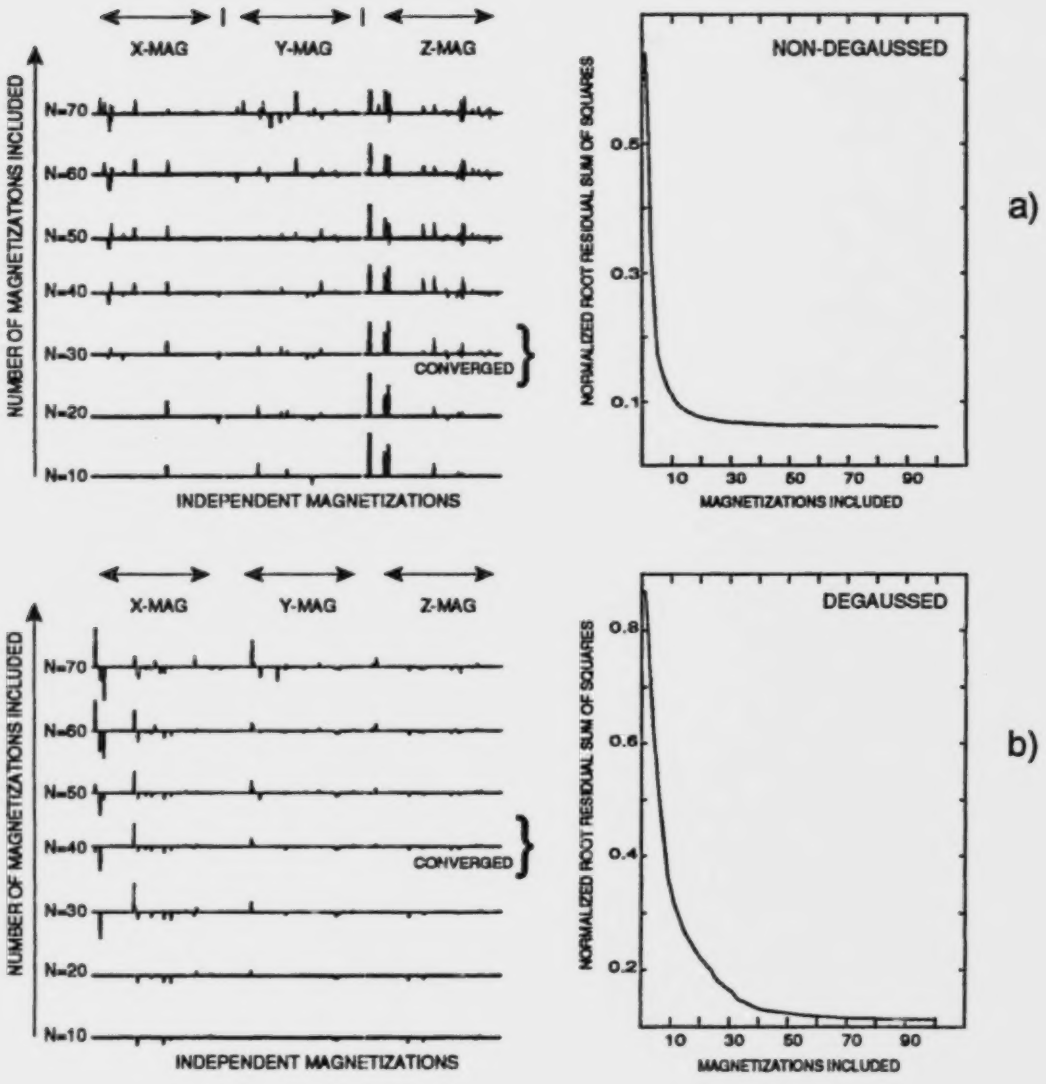

Figure 9: One-spike-at-a-time technique applied to a) a non-degaussed, and b) degaussed vessel, showing both the evolution of the weights and the square-root of the residual square error.

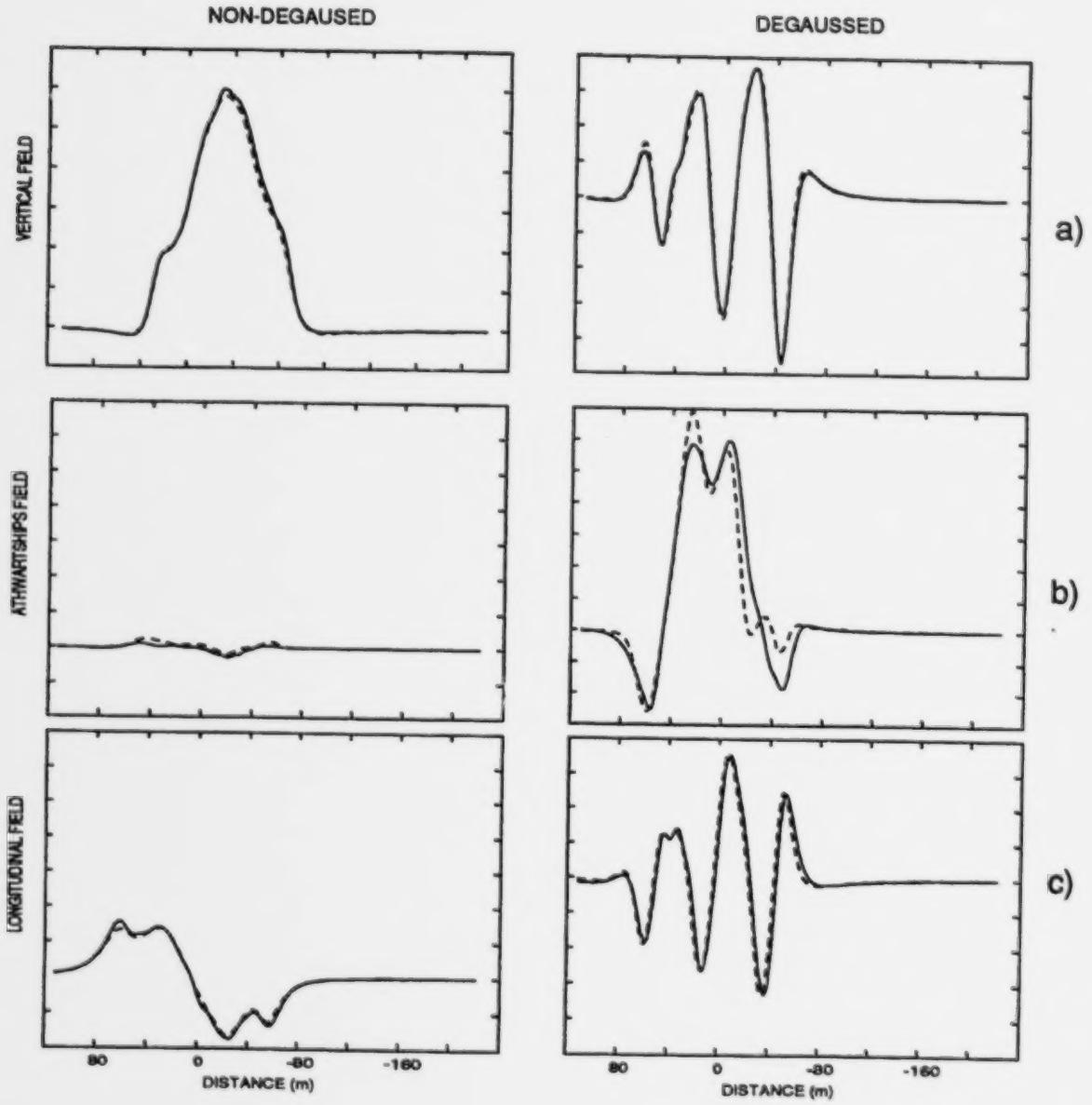

Figure 10: A comparison of the measured (solid line) and modelled (dashed) a) vertical, b) athwartships and c) longitudinal keel-line signatures.

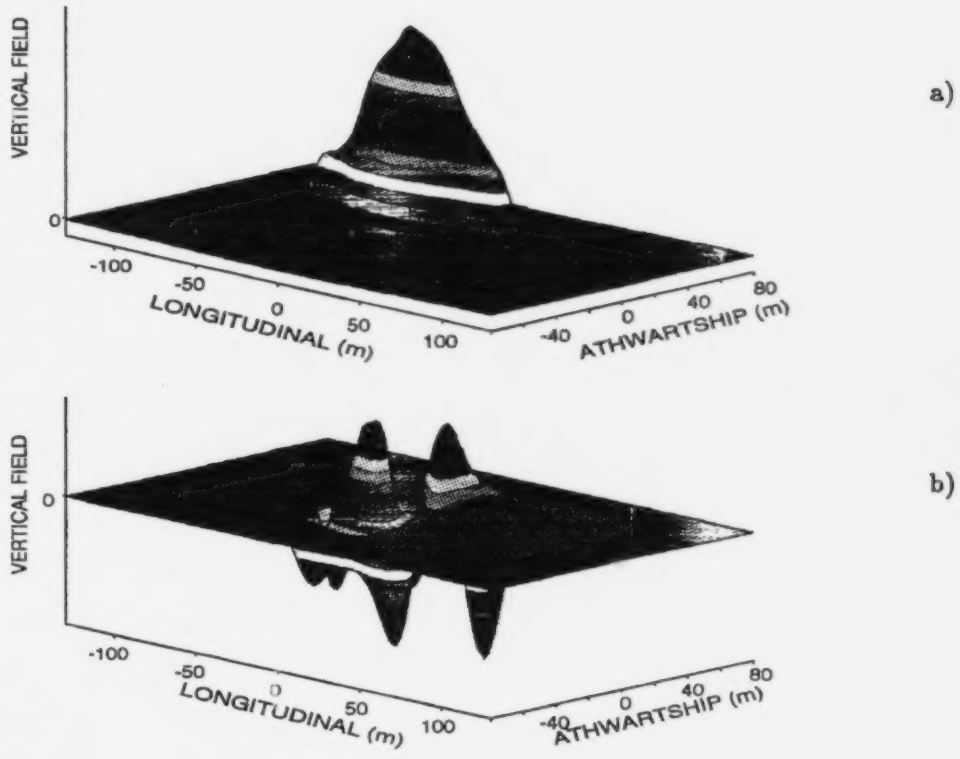

Figure 11: The modelled vertical magnetic field signatures for the a) non-degaussed, and b) degaussed vessel.

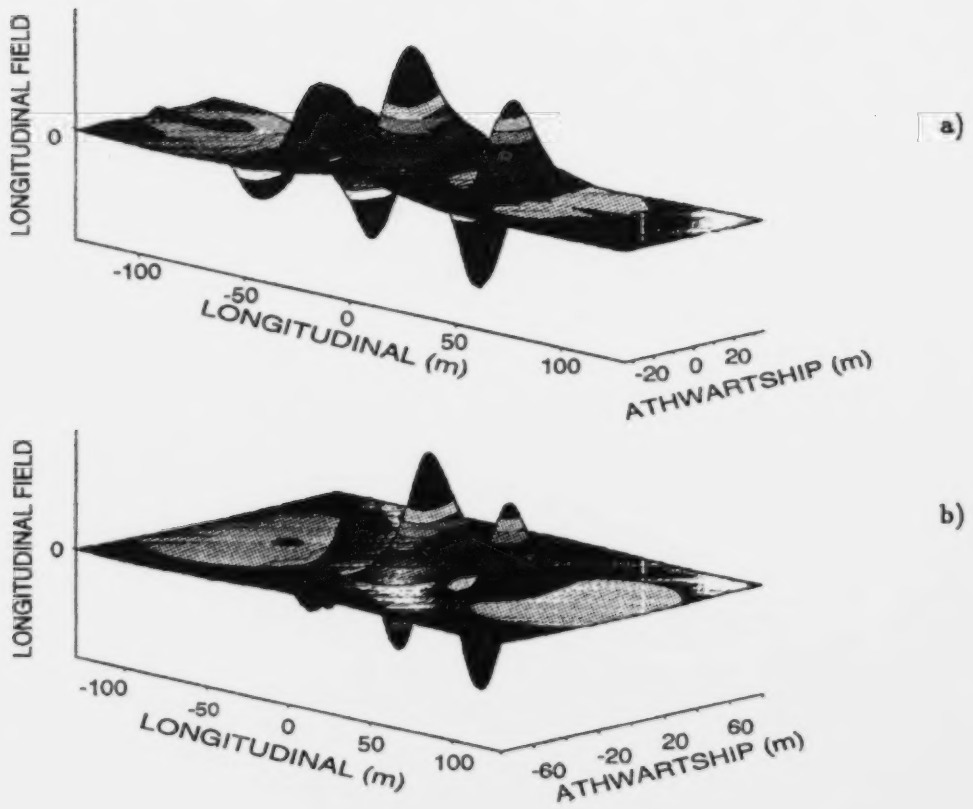

Figure 12: A comparison of the a) experimental, and b) modelled longitudinal magnetic field for the degaussed vessel.

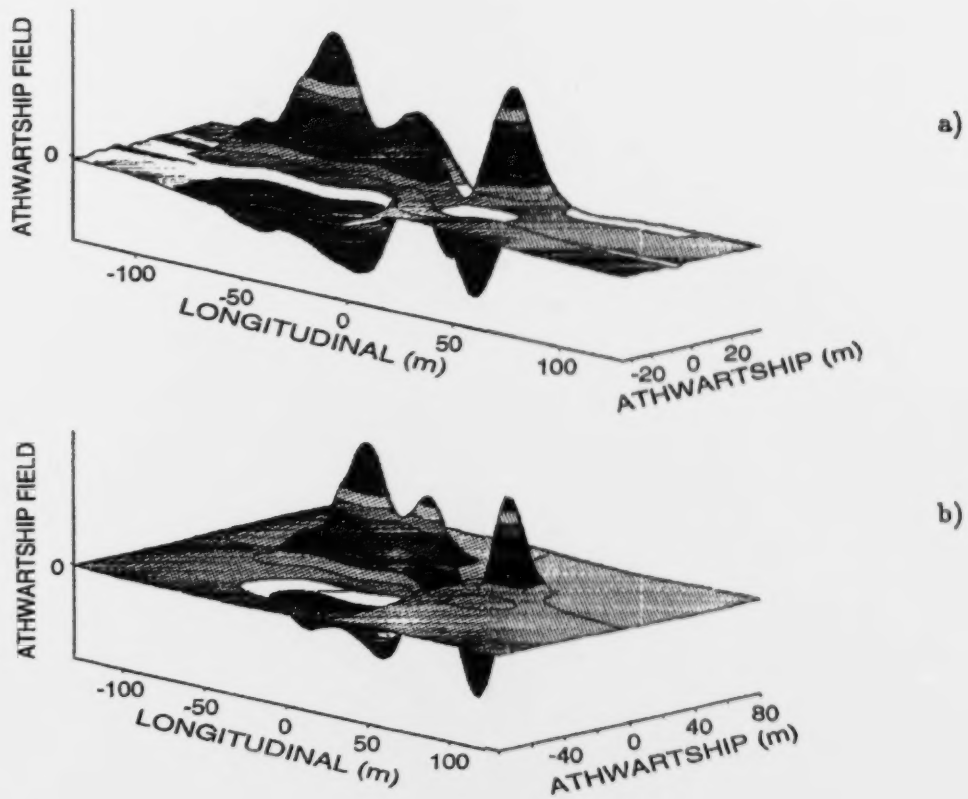

Figure 13: A comparison of the a) experimental, and b) modelled athwartships magnetic field for the degaussed vessel.

clearly the solution to $\underset{\approx}{E}(\underset{\sim}{p})_f \underset{\sim}{w}_f \approx \underset{\sim}{B}^{meas}$, where the notation $\underset{\approx}{E}(\underset{\sim}{p})_f$ implies that $\underset{\approx}{E}_f$ is a function of the position and focal length values stored in the $4f \times 1$ column vector $\underset{\sim}{p}$.

If we define an error vector $\underset{\sim}{\epsilon}(\underset{\sim}{p}) = \underset{\approx}{E}(\underset{\sim}{p})_f \underset{\sim}{w}_f - \underset{\sim}{B}^{meas}$, and an error function $J(\underset{\sim}{p}) = \underset{\sim}{\epsilon}^T \underset{\sim}{\epsilon}$, then we wish to minimize $J(\underset{\sim}{p})$ with respect to $\underset{\sim}{p}$. Differentiating, and setting equal to zero, we have

$$\frac{\partial J(\underset{\sim}{p})}{\partial \underset{\sim}{p}} = 2\, \underset{\approx}{D}^T \underset{\sim}{\epsilon}(\underset{\sim}{p}) = \underset{\sim}{0} \tag{55}$$

where $\partial J / \partial \underset{\sim}{p}$ is a $4f \times 1$ column vector and where the *derivative matrix* $\underset{\approx}{D}$ is the $3m \times 4f$ matrix

$$\underset{\approx}{D}(\underset{\sim}{p}) = \frac{\partial \underset{\sim}{\epsilon}}{\partial \underset{\sim}{p}} \quad \text{with components} \quad D_{ij} = \frac{\partial \epsilon_i}{\partial p_j} \tag{56}$$

To solve for the new position vector $\underset{\sim}{p}$ we expand $\underset{\sim}{\epsilon}(\underset{\sim}{p})$ using a Taylor series about the initial vector $\underset{\sim}{p} = \underset{\sim}{p}_0$ to give

$$2\, \underset{\approx}{D}^T \left[\underset{\sim}{\epsilon}(\underset{\sim}{p}_0) + \underset{\approx}{D}(\underset{\sim}{p}_0)\, \Delta \underset{\sim}{p} \right] \approx \underset{\sim}{0} \tag{57}$$

where we have assumed the initial fit is sufficiently close that only the first two terms of the expansion need be retained. The new position vector is then given by

$$\underset{\sim}{p} = \underset{\sim}{p}_0 + \Delta \underset{\sim}{p} \tag{58}$$

where $\Delta \underset{\sim}{p}$ is found by solving

$$\underset{\approx}{D}(\underset{\sim}{p}_0)\, \Delta \underset{\sim}{p} \approx - \underset{\sim}{\epsilon}(\underset{\sim}{p}) \tag{59}$$

The original model equation $\underset{\approx}{E} \underset{\sim}{w} = \underset{\sim}{B}^{meas}$ can now be solved for the new position vector $\underset{\sim}{p}$, and the error function recomputed. If J has decreased, the procedure has been worthwhile and can be reiterated as appropriate. The derivative matrix $\underset{\approx}{D}$ can be evaluated by writing the error vector $\underset{\sim}{\epsilon}$ in terms of the rows $\underset{\sim}{R}_i^T$ of $\underset{\approx}{E}_f$ to yield

$$\epsilon_i = \underset{\sim}{R}_i^T \underset{\sim}{w} - B_i^{meas} \tag{60}$$

and thus

$$D_{ij} = \frac{\partial \epsilon_i}{\partial p_j} = \frac{\partial}{\partial p_j} \underset{\sim i}{R}^T \underset{\sim}{w} = \frac{\partial}{\partial p_j} \sum_k \left(\underset{\sim i}{R}^T(\underset{\sim}{p}) \right)_k (\underset{\sim}{w})_k \delta_{\beta_1 \beta_2} \quad \text{where} \quad i \subset \alpha,\ j \subset \beta_1,\ k \subset \beta_2 \qquad (61)$$

where we have re-introduced the α, β notation of Section 5.1. The δ-function indicates that for any measurement location α where $i \subset \alpha$, the only columns of $\underset{\sim i}{R}^T(\underset{\sim}{p})$ that contribute to the summation are those four that correspond to the same source site as does the parameter that is being differentiated with respect to. These derivatives are evaluated in Appendix C.

Initial attempts to solve (59) using least-squares techniques led to oscillation problems similar to those found in Section 2, but application of the one-spike-at-a-time method gave physically realistic coordinate shifts. Once again, the number or spikes (or in this case coordinate shifts) used in the technique was assessed subjectively by observing the solutions and the error function, since too many spikes caused the onset of oscillations.

An evaluation of the position optimization technique for several true signatures, showed that although the *r.m.s.* error was invariably reduced, the decrease was only in the order of 0.5 to 1.0%, a result we suspect arose from the large number of spheroids used in our model. We also found that there were only occasional variations in c, suggesting that our original spheroids were appropriately sized. We would imagine that for models where considerably fewer sources were used, or perhaps for GRP hulls where the magnetization is more discretely localized, the improvements through position optimisation would be greater. We note that the technique was originally introduced by Yan *et al.* for models that used just a limited number of spheroids.

9 CONCLUDING REMARKS AND SUMMARY

The present report has shown that the non-physical oscillating solutions obtained during some simple least-squares approaches to magnetic modelling arise from the rank deficiency of the model matrix linking the source-functions to the predicted magnetic field. These problems are exacerbated when the number of sources is increased in an attempt to improve the fit to a complex field and source distribution. The sources become covariant, implying that several or many sources can contribute almost equally to the predicted field. Singular value decomposition showed that, although the original simultaneous equations describing the representation might have been thought to be over-determined, due to the large number of magnetic field values typically used during a fit, this source covariance led to the problem being under-determined. This in turn results in there being a multitude of non-unique source distributions that can each describe the data within some least-squares sense. The particular form of the solution being returned depends on the mechanics of the calculation, together with the experimental and computational sources of noise.

An approach was presented that represented the magnetization of a vessel by a series of magnetized prolate spheroids. Such a representation can use fewer sources than a simple multi-dipole

representation, yet at the same time can populate the entire volume of the vessel. The prolate spheroid equations were extended from the original work of Yan *et al.*[1] to show that permanent, induced and combined sources of magnetization could be described by the same model. When used with an adapted form of a one-spike-at-a-time fitting technique, in which source site magnetizations are determined individually rather than being deduced simultaneously as in standard least-squares techniques, the problems of oscillatory solutions were essentially eliminated, and a sparse physically realistic solution returned. During tests on a variety of ship signatures, the model has had a high degree of faithfulness, and has proved quite successful in modelling magnetic signatures for our mine simulation studies.

In conclusion we should point out that in its present form, the implementations of both the prolate spheroid model and the one-spike-at-a-time technique were intended for non real-time applications, such as the retroactive fitting to range data and the subsequent estimation of ship signatures. Current research is investigating the use of parallel architecture and algorithm refinement to make the approach more suited to real-time applications. It is also suspected that the one-spike-at-a-time approach may be of benefit to a variety of other magnetic modelling techniques. The results of a study of its use in monopole, standard-dipole and current-loop modelling will be presented at a later date.

A APPENDIX A

The following sections derive solutions of the simultaneous equations

$$\underset{\sim}{B}^{meas} \approx \underset{\approx}{E}\underset{\sim}{w} \tag{A2}$$

for both full rank and rank-deficient matrices $\underset{\approx}{E}$.

A.1 STANDARD LEAST SQUARES

The standard least-squares (full rank) solution is found by determining the vector $\underset{\sim}{w}=\underset{\sim}{w}^{STD}$ that minimizes the sum of residuals

$$\| \underset{\sim}{B}^{meas} - \underset{\approx}{E}\underset{\sim}{w} \|_2^2 = (\underset{\sim}{B}^{meas} - \underset{\approx}{E}\underset{\sim}{w})^T(\underset{\sim}{B}^{meas} - \underset{\approx}{E}\underset{\sim}{w}) = min. \tag{A3}$$

For this to be true, we must have

$$\| \underset{\sim}{B}^{meas} - \underset{\approx}{E}\,(\underset{\sim}{w}^{STD} + \underset{\sim}{\epsilon})\|_2^2 - \| \underset{\sim}{B}^{meas} - \underset{\approx}{E}\underset{\sim}{w}^{STD} \|_2^2 > 0 \tag{A4}$$

for any vector $\underset{\sim}{\epsilon}$. Straight forward expansion followed by re-arrangement leads to

$$\underset{\sim}{\epsilon}^T (\underset{\approx}{E}^T\underset{\approx}{E}\underset{\sim}{w} - \underset{\approx}{E}^T\underset{\sim}{B}^{meas}) + (\underset{\sim}{w}^T\underset{\approx}{E}^T\underset{\approx}{E} - (\underset{\sim}{B}^{meas})^T\underset{\approx}{E})\,\underset{\sim}{\epsilon} + \underset{\sim}{\epsilon}^T\underset{\approx}{E}^T\underset{\approx}{E}\underset{\sim}{\epsilon} > 0 \tag{A5}$$

Noting the first two terms are identical scalars of indeterminate sign, this equality can only be true for arbitrary $\underset{\sim}{\epsilon}$ if $\underset{\approx}{E}^T\underset{\approx}{E}\underset{\sim}{w} - \underset{\approx}{E}^T\underset{\sim}{B}^{meas} = 0$. Thus the standard least-squares solution satisfies the *normal* equations

$$\underset{\approx}{E}^T\underset{\sim}{B}^{meas} = \underset{\approx}{E}^T\underset{\approx}{E}\underset{\sim}{w} \tag{A6}$$

A.2 RANK-DEFICIENT CASE

As outlined in Section 3, the solution to (A2) is not unique when $\underset{\approx}{E}$ is rank-deficient and of rank ρ. Of interest is the particular solution that satisfies

$$\| \underset{\sim}{B}^{meas} - \underset{\approx}{E}\underset{\sim}{w} \|_2^2 = min. \tag{A7}$$

and has minimum length

$$\| \underset{\sim}{w} \|_2^2 = min. \tag{A8}$$

A.2.1 MINIMUM-RESIDUAL SOLUTIONS

To obtain the solutions of minimum residual we use the same approach as for the standard least-squares case, but substitute the SVD factorization of $\underset{\approx}{E}$ (see (11)) into (A4) to obtain

$$\underset{\sim}{\epsilon}^T (\underset{\approx}{V}\underset{\approx}{\Sigma}^T\underset{\approx}{U}^T\underset{\approx}{U}\underset{\approx}{\Sigma}\underset{\approx}{V}^T\underset{\sim}{w} - \underset{\approx}{V}\underset{\approx}{\Sigma}^T\underset{\approx}{U}^T\underset{\sim}{B}^{meas}) \; +$$

$$(\underset{\sim}{w}^T\underset{\approx}{V}\underset{\approx}{\Sigma}^T\underset{\approx}{U}^T\underset{\approx}{U}\underset{\approx}{\Sigma}\underset{\approx}{V}^T - (\underset{\sim}{B}^{meas})^T\underset{\approx}{U}\underset{\approx}{\Sigma}\underset{\approx}{V}^T)\,\underset{\sim}{\epsilon} \; + \; \underset{\sim}{\epsilon}^T\underset{\approx}{V}\underset{\approx}{\Sigma}^T\underset{\approx}{U}^T\underset{\approx}{U}\underset{\approx}{\Sigma}\underset{\approx}{V}^T\underset{\sim}{\epsilon} > 0 \tag{A9}$$

As before, the first two terms are identical sign-indeterminate scalars, and the relationship can only be satisfied for arbitrary $\underset{\sim}{\epsilon}$ if $\underset{\approx}{V}\underset{\approx}{\Sigma}^T\underset{\approx}{U}^T\underset{\approx}{U}\underset{\approx}{\Sigma}\underset{\approx}{V}^T\underset{\sim}{w} = \underset{\approx}{V}\underset{\approx}{\Sigma}^T\underset{\approx}{U}^T\underset{\sim}{B}^{meas}$. Premultiplication by $\underset{\approx}{V}^T$ and simplification through use of the properties (12) leads to

$$\underset{\approx}{\Sigma}^T\underset{\approx}{\Sigma}\underset{\approx}{V}^T\underset{\sim}{w} = \underset{\approx}{\Sigma}^T\underset{\approx}{U}^T\underset{\sim}{B}^{meas} \tag{A10}$$

which, when $\underset{\approx}{E}$ is rank-deficient can be written

$$\underset{\approx_\rho}{\Sigma}^T\underset{\approx_\rho}{\Sigma}\,\underset{\approx_\rho}{V}^T\underset{\sim}{w} = \underset{\approx_\rho}{\Sigma}^T\underset{\approx_\rho}{U}^T\underset{\sim}{B}^{meas} \tag{A11}$$

where the submatrices denoted by the subscript ρ were defined in Section 4.1. Since $\underset{\approx_\rho}{\Sigma}$ (which is identical to $\underset{\approx_\rho}{\Sigma}^T$) is a square diagonal matrix with non-vanishing trace, its inverse exists which enables (A11) to be solved to give

$$\underset{\sim}{w}^{SVD} = \underset{\approx_\rho}{V}\underset{\approx_\rho}{\Sigma}^{-1}\underset{\approx_\rho}{U}^T\underset{\sim}{B}^{meas} \tag{A12}$$

where $\underset{\approx_\rho}{\Sigma}^{-1}$ has solely the diagonal elements $\{\sigma_i^{-1} \;\; for \; i = 1 \ldots \rho\}$. Straightforward multiplication yields the equivalent form $\underset{\sim}{w}^{SVD} = \underset{\approx}{E}^+\underset{\sim}{B}^{meas} = \underset{\approx}{V}\underset{\approx}{\Sigma}^+\underset{\approx}{U}^T\underset{\sim}{B}^{meas}$ where $\underset{\approx}{E}^+$ is the pseudo-inverse of $\underset{\approx}{E}$ described earlier.

It can also be seen that the vector formed by adding any solution $\underset{\sim}{w}^{HOM}$ of the homogeneous equation $\underset{\approx}{E}\underset{\sim}{w} = \underset{\approx}{0}$ to $\underset{\sim}{w}^{SVD}$ satisfies (A7), since substitution into (A10) leads to an extra quantity $\underset{\approx}{\Sigma}^T\underset{\approx}{\Sigma}\underset{\approx}{V}^T\underset{\sim}{w}^{HOM}$ on the left-hand side, which, after using the identity $\underset{\approx}{\Sigma}^T\underset{\approx}{U}^T\underset{\approx}{U}\underset{\approx}{\Sigma}=\underset{\approx}{\Sigma}^T\underset{\approx}{\Sigma}$ since $\underset{\approx}{U}^T\underset{\approx}{U}=\underset{\approx}{I}$, becomes

$$\underset{\approx}{\Sigma}^T\underset{\approx}{U}^T\underset{\approx}{U}\underset{\approx}{\Sigma}\underset{\approx}{V}^T\underset{\sim}{w}^{HOM} = \underset{\approx}{\Sigma}^T\underset{\approx}{U}^T\underset{\approx}{E}\underset{\sim}{w}^{HOM} \tag{A13}$$

and equal to zero by definition of $\underset{\sim}{w}^{HOM}$.

Consequently the solutions of the minimal-residuals equation (A7) are given by the infinite set of vectors $\underset{\sim}{w}^{SVD} + \underset{\sim}{w}^{HOM}$. These are, of course, the non-unique solutions described earlier.

A.2.2 MINIMUM-LENGTH SOLUTION

To prove that the SVD-solution is the smallest of the minimal-residual solutions derived above, we expand $\| \underset{\sim}{w}^{SVD} + \underset{\sim}{w}^{HOM} \|_2^2$ to give

$$(\underset{\sim}{w}^{SVD})^T\,\underset{\sim}{w}^{SVD} + 2(\underset{\sim}{w}^{HOM})^T\,\underset{\sim}{w}^{SVD} + (\underset{\sim}{w}^{HOM})^T\,\underset{\sim}{w}^{HOM} \tag{A14}$$

Focusing on the second term and dropping the factor 2 we have

$$(\underset{\sim}{w}^{HOM})^T\,\underset{\sim}{w}^{SVD} = (\underset{\sim}{w}^{HOM})^T\,\underset{\approx}{E}^{+}\underset{\sim}{B}^{meas} = (\underset{\sim}{w}^{HOM})^T\,\underset{\approx}{V}\underset{\approx}{\Sigma}^{+}\underset{\approx}{U}^T\underset{\sim}{B}^{meas} \tag{A15}$$

which on evaluating $\underset{\approx}{V}\underset{\approx}{\Sigma}^{+}$ becomes

$$(\underset{\sim}{w}^{HOM})^T\left(\sigma_1^{-1}\,\underset{\sim}{v}_1 \quad \sigma_2^{-1}\,\underset{\sim}{v}_2 \quad \sigma_3^{-1}\,\underset{\sim}{v}_3 \quad \ldots \quad \sigma_\rho^{-1}\,\underset{\sim}{v}_\rho \quad \underset{\approx}{0}^{[3n:3m-\rho]}\right)\underset{\approx}{U}^T\underset{\sim}{B}^{meas} \tag{A16}$$

where the $\underset{\sim}{v}_i$ are the first ρ column-vectors of $\underset{\approx}{V}$, and $\underset{\approx}{0}^{[3n:3m-\rho]}$ is a $3n \times 3m-\rho$ null matrix. Substitution of the SVD-factorization for $\underset{\approx}{E}$ into the homogeneous equation, followed by premultiplication by $\underset{\approx}{U}^T$ leads to

$$\underset{\approx}{\Sigma}\underset{\approx}{V}^T\underset{\sim}{w}^{HOM} = \underset{\approx}{0}^{[3m:1]} \tag{A17}$$

which after transposing and evaluating the product $\underset{\approx}{V}\underset{\approx}{\Sigma}^T$ yields

$$(\underset{\sim}{w}^{HOM})^T \left(\sigma_1 \underset{\sim}{v}_1 \quad \sigma_2 \underset{\sim}{v}_2 \quad \sigma_3 \underset{\sim}{v}_3 \quad \cdots \quad \sigma_\rho \underset{\sim}{v}_\rho \quad \underset{\approx}{0}^{[3n:3m-\rho]} \right) = \underset{\approx}{0}^{[1:3m]} \tag{A18}$$

showing that any solution of the homogeneous equation must be orthogonal to the first ρ columns of $\underset{\approx}{V}$ *ie.* $(\underset{\sim}{w}^{HOM})^T \underset{\sim}{v}_i = 0$ *for* $i = 1 \ldots \rho$. Utilizing this fact in (A18) leads to the orthogonality relationship $(\underset{\sim}{w}^{HOM})^T \underset{\sim}{w}^{SVD} = 0$ and hence

$$\| \underset{\sim}{w}^{SVD} + \underset{\sim}{w}^{HOM} \|_2^2 = \| \underset{\sim}{w}^{SVD} \|_2^2 + \| \underset{\sim}{w}^{HOM} \|_2^2 \tag{A19}$$

thus proving, since $\| \underset{\sim}{w}^{HOM} \|_2^2$ is a positive-definite scalar, that the SVD-solution is the solution of smallest length.

B FIELDS OF A MAGNETIZED PROLATE SPHEROID

The following sections derive solutions of Laplace's equation for prolate spheroids of either permanent or induced magnetization, or for combinations of both, and polarized in any of the three principal directions.

B.1 BACKGROUND

In Section 3.2 the magnetic field produced by a uniformly magnetized prolate spheroid was written as the gradient of a magnetic scalar potential Ψ, *i.e.*

$$\vec{H} = -\vec{\nabla}\Psi \tag{B20}$$

which satisfied Laplace's equation

$$\nabla^2\Psi = 0 \tag{B21}$$

The induction is related to the magnetic field within the spheroid by the usual relationship $\vec{B}_{in} = \mu_0(\vec{H}_{in} + \vec{M})$, and outside, where $\vec{M} = 0$, by $\vec{B}_{out} = \mu_0\vec{H}_{out}$

The equations are best solved by changing to the prolate spheroidal co-ordinate system (ξ, η, ϕ) (with origin at the spheroid centre)

$$\xi = \left\{\sqrt{(x+c)^2+y^2+z^2} - \sqrt{(x-c)^2+y^2+z^2}\right\}/(2c) \tag{B22}$$

$$\eta = \left\{\sqrt{(x+c)^2+y^2+z^2} + \sqrt{(x-c)^2+y^2+z^2}\right\}/(2c) \tag{B23}$$

$$\text{and} \quad \phi = \tan^{-1}(y/z) \tag{B24}$$

where

$$c = \sqrt{a^2-b^2} \tag{B25}$$

and where a and b are semi-major and semi-minor radii of the spheroid respectively. The co-ordinate ranges are

$$1 \le \eta \le \infty \qquad -1 \le \xi \le 1 \qquad \text{and} \quad 0 \le \phi \le 2\pi \tag{B26}$$

Squaring (B23) followed by some re-arrangement leads to

$$\left[2c^2\eta^2 - (x^2+y^2+z^2+c^2)\right] = \sqrt{(x^2+y^2+z^2+c^2)^2 - 4x^2c^2} \tag{B27}$$

which on re-squaring and further re-arrangement yields

$$\frac{x^2}{\eta^2} + \frac{y^2}{\eta^2-1} + \frac{z^2}{\eta^2-1} = c^2 \tag{B28}$$

The surface $\eta = \eta_0 = constant$ is thus a prolate spheroid with interfocal distance $2c$, major axis $c\eta_0$, and minor axis $c\sqrt{\eta_0^2-1}$.

The inverses of (B22)-(B24) can be written

$$x = c\eta\xi \tag{B29}$$

$$y = c\sqrt{(\eta^2-1)(1-\xi^2)}\sin\phi \tag{B30}$$

$$z = c\sqrt{(\eta^2-1)(1-\xi^2)}\cos\phi \tag{B31}$$

Once Ψ has been determined, the magnetic field can be written in Cartesian co-ordinates using (B20) where

$$\frac{\partial\Psi}{\partial x_i} = \frac{\partial\xi}{\partial x_i}\frac{\partial\Psi}{\partial\xi} + \frac{\partial\eta}{\partial x_i}\frac{\partial\Psi}{\partial\eta} + \frac{\partial\phi}{\partial x_i}\frac{\partial\Psi}{\partial\phi} \tag{B32}$$

and x_i is any one of (x,y,z).

The required derivatives of η and ξ can be calculated from (B22-B24) and shown to be

$$\frac{\partial\xi}{\partial x} = \eta\,\frac{1-\xi^2}{\eta^2-\xi^2}\frac{1}{c} \qquad \frac{\partial\xi}{\partial y} = -\xi\,\frac{y/c^2}{\eta^2-\xi^2} \tag{B33}$$

$$\frac{\partial\eta}{\partial x} = \xi\,\frac{\eta^2-1}{\eta^2-\xi^2}\frac{1}{c} \qquad \frac{\partial\eta}{\partial y} = \eta\,\frac{y/c^2}{\eta^2-\xi^2} \tag{B34}$$

with the z derivatives being obtained by interchange of y and z. The derivatives of ϕ are given by

$$\frac{\partial \phi}{\partial x} = 0 \qquad \frac{\partial \phi}{\partial y} = \frac{1}{1 + (y/z)^2} \frac{1}{z} \qquad \frac{\partial \phi}{\partial z} = \frac{-1}{1 + (y/z)^2} \frac{y}{z^2} \tag{B35}$$

where y and z are given above.

The general solution to Laplace's equation *outside* of the spheroid was found by separation of variables to be

$$\Psi^{out} = \sum_n \sum_m \{a_{nm} P_n^m(\xi) + b_{nm} Q_n^m(\xi)\} [c_{nm} P_n^m(\eta) + d_{nm} Q_n^m(\eta)] \{e_m \cos m\phi + f_m \sin m\phi\} \tag{B36}$$

where P_n^m and Q_n^m were the associated Legendre functions of the 1st and 2nd kind respectively, and where a,b,c,d,e and f were arbitrary coefficients, which must be determined by considerations of symmetry and finiteness, and by matching boundary conditions on the surface of the spheroid. Consideration of $Q_n^m(\xi)$ at $\xi = \pm 1$, and $P_n^m(\eta)$ as $\eta \to \infty$ led to $b_{nm} = c_{nm} = 0$, so that

$$\Psi^{out} = \sum_n \sum_m b_{nm} P_n^m(\xi) Q_n^m(\eta) \{e_m \cos m\phi + \sin m\phi\} \tag{B37}$$

where the arbitrary coefficient b_{nm} has been redefined and a further coefficient e_m introduced.

For convenience, at this point, we introduce the specific forms for the Legendre functions

$$P_1^0(\xi) = \xi \tag{B38}$$

$$Q_1^0(\eta) = \frac{1}{2} \eta \, \ell n \frac{\eta + 1}{\eta - 1} - 1 \tag{B39}$$

$$P_1^1(\xi) = \sqrt{1 - \xi^2} \tag{B40}$$

and

$$Q_1^1(\eta) = \frac{\eta}{\sqrt{\eta^2 - 1}} - \sqrt{\eta^2 - 1} \frac{1}{2} \ell n \frac{\eta + 1}{\eta - 1} \tag{B41}$$

B.2 PERMANENT MAGNETIZATION

B.2.1 LONGITUDINAL

In the absence of an externally applied field, and if the longitudinal magnetization of the spheroid is homogeneous, the internal magnetic properties are described by $\vec{M} = (M, 0, 0)$, $\vec{B}_{in} = (B_{in}, 0, 0)$, $\vec{H}_{in} = (H_{in}, 0, 0)$, and $B_{in} = \mu_0(H_{in} + M)$. Since H_{in} and M are related by $H_{in} = -N_L M$, where N_L is the longitudinal demagnetizing factor, the induction can be rewritten

$$B_{in} = \mu_0(H_{in} + M) = \mu_0(1 - N_L)M = \mu_0(1 - N_L^{-1})H_{in} \tag{B42}$$

Laplace's equation can now be solved to give

$$\Psi^{in} = -H_{in}x = N_L M x = N_L M c\xi\eta \tag{B43}$$

Outside of the spheroid, due to the cylindrical symmetry, Ψ has no ϕ-dependence, so that the m-summation in (B37) can be restricted to $m = 0$ yielding

$$\Psi^{out} = \sum_{n=0}^{\infty} b_n P_n^0(\xi) Q_n^0(\eta) \tag{B44}$$

In the new coordinates, the tangential field-component H_{tang} is given by $H_{tang} = -\lambda_\xi^{-1}\partial\Psi/\partial\xi$ where λ_ξ is one of the usual scaling factors $(\lambda_\xi, \lambda_\eta, \lambda_\phi)$ associated with any change in co-ordinate system.[10] Applying continuity to this tangential component across the spheroid boundary at $\eta = \eta_0$ we find

$$\left.\frac{\partial\Psi^{in}}{\partial\xi}\right|_{\eta=\eta_0} = \left.\frac{\partial\Psi^{out}}{\partial\xi}\right|_{\eta=\eta_0} \quad \text{or} \quad N_L M c\eta_0 = \sum_{n=0}^{\infty} b_n \frac{\partial P_n^0(\xi)}{\partial\xi} Q_n^0(\eta_0) \tag{B45}$$

Clearly this can only be satisfied for arbitrary ξ if all the b_n vanish except for b_1, which leads to the result

$$\Psi^{out} = \frac{N_L M c\eta_0}{Q_1^0(\eta_0)} P_1^0(\xi) Q_1^0(\eta) \tag{B46}$$

To determine and then eliminate the demagnetizing factor we apply continuity to the normal component of $\vec{B}$ at the surface. Using $H_{norm} = -\lambda_\eta^{-1}\partial\Psi/\partial\eta$ together with (B42), (B43), (B46) and (B38), and noting that outside the spheroid $M = 0$ so that $\vec{B}_{out} = \mu_0\vec{H}_{out}$, we find

$$(1 - N_L)Mc\xi|_{\eta=\eta_0} = -\frac{N_L M c\eta_0}{Q_1^0(\eta_0)} \xi \left.\frac{\partial Q_1^0(\eta)}{\partial\eta}\right|_{\eta=\eta_0} \tag{B47}$$

[10] See e.g. Morse and Feschbach[8].

which, on utilising (B39) to evaluate $\partial Q_1^0(\eta)/\partial\eta$ leads to

$$N_L = (\eta_0^2 - 1)Q_1^0(\eta_0) \tag{B48}$$

Substituting for N_L into (B46) yields

$$\Psi^{out}(\xi,\eta) = (\eta_0^2 - 1)\eta_0 Mc P_1^0(\xi)Q_1^0(\eta) \equiv (\eta_0^2 - 1)\eta_0 Mc\xi Q_1^0(\eta) \tag{B49}$$

B.2.2 TRANSVERSE

If the spheroid magnetization is polarized along the y-direction, the expressions for the internal magnetic properties become $\vec{M} = (0, M, 0)$, $\vec{B}_{in} = (0, B_{in}, 0)$, $\vec{H}_{in} = (0, H_{in}, 0)$, $B_{in} = \mu_0(H_{in} + M)$, and $H_{in} = -N_T M$, where N_T is now the transverse demagnetizing factor. The induction relationship becomes

$$B_{in} = \mu_0(H_{in} + M) = \mu_0(1 - N_T)M = \mu_0(1 - N_T^{-1})H_{in} \tag{B50}$$

and the solution to Laplace's equation becomes

$$\Psi^{in} = -H_{in}y = N_T My = N_T Mc\sqrt{(1-\xi^2)(\eta^2-1)}\sin\phi \tag{B51}$$

The mirror-plane symmetry restricts the m-summation in (B37) to $m = 1$ so that the external potential can be written

$$\Psi^{out} = \sum_{n=0}^{\infty} b_n P_n^1(\xi)Q_n^1(\eta)(\sin\phi + e_1\cos\phi) \tag{B52}$$

Following the technique of the previous section, and matching $\partial\Psi/\partial\xi$ at $\eta = \eta_0$ to ensure continuity[11] of the tangential component of $\vec{H}$ at the spheroid surface, leads to

$$\Psi^{out} = \frac{N_T Mc\sqrt{\eta_0^2 - 1}}{Q_1^1(\eta_0)} P_1^1(\xi)Q_1^1(\eta)\sin\phi \tag{B53}$$

The transverse demagnetizing factor can be determined by matching the normal component of $\vec{B}$ at the spheroid surface, which amounts to equating $(1 - N_T^{-1})\partial\Psi^{in}/\partial\eta$ and $\partial\Psi^{out}/\partial\eta$ at $\eta = \eta_0$. After calculating $\partial Q_1^1(\eta)/\partial\eta$ from (B41), and some re-arrangement we arrive at

$$N_T = \frac{1}{2}Q_1^1(\eta_0)\eta_0\sqrt{\eta_0^2 - 1} \tag{B54}$$

[11] Matching also shows e_1 to be zero.

which on substituting into (B53) leads to

$$\Psi^{out} = \frac{1}{2}\eta_0(\eta_0^2-1)McP_1^1(\xi)Q_1^1(\eta)\sin\phi = \frac{1}{2}\eta_0(\eta_0^2-1)Mc\sqrt{1-\xi^2}Q_1^1(\eta)\sin\phi \tag{B55}$$

B.3 INDUCED MAGNETIZATION

B.3.1 LONGITUDINAL

When there is no permanent magnetization, and the spheroid is subject to an applied longitudinal field H_0, the internal magnetic properties must be written as $\vec{M} = (M,0,0)$, $\vec{B}_{in} = (B_{in},0,0)$, $\vec{H}_{in} = (H_{in},0,0)$, and $B_{in} = \mu_0(H_{in}+M)$, but now with $M = \chi H_{in}$ where χ is the magnetic susceptibility. The remaining relationships become

$$H_{in} = H_0 - N_L M = H_{in} = H_0/(1+\chi N_L) \tag{B56}$$

and the internal induction can be written

$$B_{in} = \mu_0(H_{in}+M) = \mu_0(1+\chi)H_{in} = \mu_0 H_0(1+\chi)/(1+\chi N_L) \tag{B57}$$

Using the result (B44) and allowing for the applied field enables Ψ^{out} to be written

$$\Psi^{out} = \sum_{n=0}^{\infty} b_n P_n^0(\xi)Q_n^0(\eta) - cH_0\eta\xi \tag{B58}$$

Applying the continuity of H_{tang} by matching $\partial\Psi/\partial\xi$ at $\eta = \eta_0$ once again leads to b_1 being the only non-vanishing coefficient, and

$$\Psi^{out} = H_0\frac{c\eta_0}{Q_1^0(\eta_0)}\frac{\chi N_L}{1+\chi N_L}P_1^0(\xi)Q_1^0(\eta) - cH_0\xi\eta \tag{B59}$$

Since the demagnetizing coefficient depends solely on geometry, N_L can be taken from Section B.2.1[12] to yield

$$\Psi^{out} = H_0\frac{c\eta_0\chi(\eta_0^2-1)}{1+\chi(\eta_0^2-1)Q_1^0(\eta_0)}P_1^0(\xi)Q_1^0(\eta) - cH_0\xi\eta \tag{B60}$$

[12]This may also be proved by considering the continuity of B_{norm} by equating $\partial\Psi^{out}/\partial\eta$ and $(1+\chi)\partial\Psi^{in}/\partial\eta$ at $\eta = \eta_0$.

B.3.2 TRANSVERSE

When the external field and induced magnetization are transverse to the spheroid, the internal equations become $\vec{M} = (0, M, 0)$, $\vec{B}_{in} = (0, B_{in}, 0)$, $\vec{H}_{in} = (0, H_{in}, 0)$, and $B_{in} = \mu_0(H_{in} + M)$, with

$$M = \chi H_{in} \tag{B61}$$

$$H_{in} = H_0 - N_T M = H_0/(1 + \chi N_T) \tag{B62}$$

and

$$B_{in} = \mu_0(H_{in} + M) = \mu_0(1 + \chi)H_{in} = \mu_0 H_0(1 + \chi)/(1 + \chi N_T) \tag{B63}$$

Using the earlier transverse general solution (B52) and adding $\vec{H}_0$ leads to

$$\Psi^{out} = \sum_{n=0}^{\infty} b_n P_n^1(\xi) Q_n^1(\eta) \sin\phi - cH_0\sqrt{(1-\xi^2)(\eta^2-1)}\sin\phi \tag{B64}$$

Matching $\partial\Psi/\partial\xi$ at $\eta = \eta_0$ leads to b_1 again being the only non-zero coefficient, and

$$\Psi^{out} = \frac{cH_0\sqrt{\eta_0^2-1}}{Q_1^1(\eta_0)} \frac{\chi N_T}{1+\chi N_T} P_1^1(\xi) Q_1^1(\eta) \sin\phi - cH_0\sqrt{(1-\xi^2)(\eta^2-1)}\sin\phi \tag{B65}$$

Taking N_T from Section B.2.2, or by equating $\partial\Psi^{out}/\partial\eta$ and $(1+\chi)\partial\Psi^{in}/\partial\eta$ at $\eta = \eta_0$, leads to

$$\Psi^{out} = \frac{cH_0\eta_0(\eta_0^2-1)\chi/2}{1+\chi Q_1^1(\eta_0)\eta_0\sqrt{\eta_0^2-1/2}} P_1^1(\xi) Q_1^1(\eta) \sin\phi - cH_0\sqrt{(1-\xi^2)(\eta^2-1)}\sin\phi \tag{B66}$$

B.4 COMBINED PERMANENT AND INDUCED

As any real vessel has both permanent and induced magnetism, we need to solve the spheroid equations for a combined magnetization $\vec{M}_P$ and $\vec{M}_I$. Four such combinations are possible:

- Both the permanent and induced moment are aligned longitudinally.
- Both the permanent and induced term are transverse to the spheroid.

- The permanent term is longitudinal whereas the induced term is transverse.
- The longitudinal term is induced and the transverse term is permanent.

which we will label I-IV.

The internal equations can be written

CASE I

$$\vec{M} = (M_P + M_I, 0, 0) \quad \vec{B}_{in} = (B_{in}, 0, 0) \quad \vec{H}_{in} = (H_{in}, 0, 0) \tag{B67}$$

$$H_{in} = H_0 - N_L(M_P + M_I) = H_0 - N_L(M_P + \chi H_{in}) = (H_0 - N_L M_P)/(1 + \chi N_L) \tag{B68}$$

$$\Psi^{in} = -x(H_0 - N_L M_P)/(1 + \chi N_L) = -c\eta\xi(H_0 - N_L M_P)/(1 + \chi N_L) \tag{B69}$$

$$\Psi^{out} = \sum_{n=0}^{\infty} b_n P_n^0(\xi) Q_n^0(\eta) - cH_0\eta\xi \tag{B70}$$

CASE II

$$\vec{M} = (0, M_P + M_I, 0) \quad \vec{B}_{in} = (0, B_{in}, 0) \quad \vec{H}_{in} = (0, H_{in}, 0) \tag{B71}$$

$$H_{in} = H_0 - N_T(M_P + M_I) = H_0 - N_T(M_P + \chi H_{in}) = (H_0 - N_T M_P)/(1 + \chi N_T) \tag{B72}$$

$$\Psi^{in} = -y(H_0 - N_T M_P)/(1 + \chi N_T) = -c\sqrt{(1 - \xi^2)(\eta^2 - 1)}\sin\phi(H_0 - N_T M_P)/(1 + \chi N_T) \tag{B73}$$

$$\Psi^{out} = \sum_{n=0}^{\infty} b_n P_n^1(\xi) Q_n^1(\eta)(\sin\phi + e_1\cos\phi) - cH_0\sqrt{(1 - \xi^2)(\eta^2 - 1)}\sin\phi \tag{B74}$$

CASE III

$$\vec{M} = (M_P, M_I, 0) \quad \vec{B}_{in} = (B_{in}^x, B_{in}^y, 0) \quad \vec{H}_{in} = (H_{in}^x, H_{in}^y, 0) \tag{B75}$$

$$H_{in}^x = -N_L M_P \quad H_{in}^y = H_0 - N_T M_I = H_0 - \chi N_T H_{in}^y = H_0/(1 + \chi N_T) \tag{B76}$$

$$B_{in}^x = \mu_0(H_{in}^x + M_P) = \mu_0(1 - N_L^{-1})H_{in}^x = \mu_0(1 - N_L)M_P \tag{B77}$$

$$B_{in}^y = \mu_0(H_{in}^y + M_I) = \mu_0(1 + \chi)H_{in}^y = \mu_0 H_0(1 + \chi)/(1 + \chi N_T) \tag{B78}$$

$$\Psi^{in} = xN_L M_P - yH_0/(1 + \chi N_T) = c\eta\xi N_L M_P - c\sqrt{(1 - \xi^2)(\eta^2 - 1)}\sin\phi H_0/(1 + \chi N_T) \tag{B79}$$

$$\Psi^{out} = \sum_{n=0}^{\infty} b_n P_n^0(\xi)Q_n^0(\eta) + \sum_{n=0}^{\infty} c_n P_n^1(\xi)Q_n^1(\eta)(\sin\phi + e_1\cos\phi) - cH_0\sqrt{(1 - \xi^2)(\eta^2 - 1)}\sin\phi \tag{B80}$$

CASE IV

$$\vec{M} = (M_I, M_P, 0) \quad \vec{B}_{in} = (B_{in}^x, B_{in}^y, 0) \quad \vec{H}_{in} = (H_{in}^x, H_{in}^y, 0) \tag{B81}$$

$$H_{in}^x = H_0 - N_L M_I = H_0 - \chi N_L H_{in}^x = H_0/(1 + \chi N_L) \tag{B82}$$

$$H_{in}^y = -N_T M_P \tag{B83}$$

$$B_{in}^x = \mu_0(H_{in}^x + M_I) = \mu_0(1 + \chi)H_{in}^x = \mu_0 H_0(1 + \chi)/(1 + \chi N_L) \tag{B84}$$

$$B_{in}^y = \mu_0(H_{in}^y + M_P) = \mu_0(1 - N_T^{-1})H_{in}^y = \mu_0(1 - N_T)M_P \tag{B85}$$

$$\Psi^{in} = -xH_0/(1+\chi N_L) + yN_T M_P = -c\eta\xi H_0/(1+\chi N_L) + c\sqrt{(1 - \xi^2)(\eta^2 - 1)}\sin\phi N_T M_P \tag{B86}$$

$$\Psi^{out} = \sum_{n=0}^{\infty} b_n P_n^0(\xi)Q_n^0(\eta) + \sum_{n=0}^{\infty} c_n P_n^1(\xi)Q_n^1(\eta)(\sin\phi + e_1\cos\phi) - cH_0\eta\xi \tag{B87}$$

Matching $\partial\Psi/\partial\xi$ at the spheroid boundary $\eta = \eta_0$ as in the previous sections leads to the external scalar potentials

$$\Psi_I^{out} = \frac{c\eta_0(\eta_0^2 - 1)(\chi H_0 + M_P)}{1 + \chi(\eta_0^2 - 1)Q_1^0(\eta_0)} P_1^0(\xi)Q_1^0(\eta) - cH_0\eta\xi \tag{B88}$$

$$\Psi_{II}^{out} = \frac{c(\eta_0^2 - 1)\eta_0(\chi H_0 + M_P)/2}{1 + \chi\eta_0\sqrt{\eta_0^2 - 1}Q_1^1(\eta_0)/2} P_1^1(\xi)Q_1^1(\eta)\sin\phi - cH_0\sqrt{(1 - \xi^2)(\eta^2 - 1)}\sin\phi \tag{B89}$$

$$\Psi_{III}^{out} = c(\eta_0^2-1)\eta_0 M_P P_1^0(\xi)Q_1^0(\eta) + \frac{c(\eta_0^2-1)\eta_0\chi H_0/2}{1+\chi\eta_0\sqrt{\eta_0^2-1}Q_1^1(\eta_0)/2} P_1^1(\xi)Q_1^1(\eta)\sin\phi$$

$$-cH_0\sqrt{(1-\xi^2)(\eta^2-1)}\sin\phi \qquad \text{(B90)}$$

$$\Psi_{IV}^{out} = \frac{c\eta_0(\eta_0^2-1)\chi H_0}{1+\chi(\eta_0^2-1)Q_1^0(\eta_0)} P_1^0(\xi)Q_1^0(\eta) + \frac{1}{2}c(\eta_0^2-1)M_P P_1^1(\xi)Q_1^1(\eta)\sin\phi - cH_0\eta\xi \qquad \text{(B91)}$$

where the demagnetizing factors N_L and N_T have been taken from (B48) and (B54).

It will be realized that just three combination equations, (Ψ_I^{out}, Ψ_{II}^{out} and a new Ψ_{III}^{out} solved for $\vec{M} = (0, 0, M_P + M_I)$) would be complete, since all other permutations could be derived by appropriate superposition, by interchange of y and z, and by setting either χ or M_P to zero as required. The four-solution approach, however, makes the following argument clearer.

B.5 SUMMARY AND COLLATION OF SOLUTIONS

The solutions for the part of scalar potential due to the spheroid alone (*i.e.* ignoring the terms $-xH_0$ or $-yH_0$ due to the external field itself, may be summarized:

LONGITUDINAL PERMANENT

$$\Psi^{out} = (\eta_0^2-1)\eta_0 McP_1^0(\xi)Q_1^0(\eta) \equiv (\eta_0^2-1)\eta_0 Mc\xi Q_1^0(\eta) \qquad \text{(B92)}$$

TRANSVERSE PERMANENT

$$\Psi^{out} = \frac{1}{2}\eta_0(\eta_0^2-1)McP_1^1(\xi)Q_1^1(\eta)\sin\phi = \frac{1}{2}\eta_0(\eta_0^2-1)Mc\sqrt{1-\xi^2}Q_1^1(\eta)\sin\phi \qquad \text{(B93)}$$

LONGITUDINAL INDUCED

$$\Psi^{out} = H_0\frac{c\eta_0\chi(\eta_0^2-1)}{1+\chi(\eta_0^2-1)Q_1^0(\eta_0)}P_1^0(\xi)Q_1^0(\eta) \qquad \text{(B94)}$$

TRANSVERSE INDUCED

$$\Psi^{out} = \frac{cH_0\eta_0(\eta_0^2-1)\chi/2}{1+\chi\eta_0\sqrt{\eta_0^2-1}Q_1^1(\eta_0)/2}P_1^1(\xi)Q_1^1(\eta)\sin\phi \qquad \text{(B95)}$$

and for the four combinations of induced and permanent magnetizations defined above

$$\Psi_I^{out} = \frac{c\eta_0(\eta_0^2-1)(\chi H_0 + M_P)}{1+\chi(\eta_0^2-1)Q_1^0(\eta_0)} P_1^0(\xi)Q_1^0(\eta) \tag{B96}$$

$$\Psi_{II}^{out} = \frac{c(\eta_0^2-1)\eta_0(\chi H_0 + M_P)/2}{1+\chi\eta_0\sqrt{\eta_0^2-1}Q_1^1(\eta_0)/2} P_1^1(\xi)Q_1^1(\eta)\sin\phi \tag{B97}$$

$$\Psi_{III}^{out} = c(\eta_0^2-1)\eta_0 M_P P_1^0(\xi)Q_1^0(\eta) + \frac{c(\eta_0^2-1)\eta_0\chi H_0/2}{1+\chi\eta_0\sqrt{\eta_0^2-1}Q_1^1(\eta_0)/2} P_1^1(\xi)Q_1^1(\eta)\sin\phi \tag{B98}$$

$$\Psi_{IV}^{out} = \frac{c\eta_0(\eta_0^2-1)\chi H_0}{1+\chi(\eta_0^2-1)Q_1^0(\eta_0)} P_1^0(\xi)Q_1^0(\eta) + \frac{1}{2}c(\eta_0^2-1)M_P P_1^1(\xi)Q_1^1(\eta)\sin\phi \tag{B99}$$

We note that each solution contains a term $\eta_0(\eta_0^2-1)$ which from (38) is related to the volume of the spheroid, indicating the *volume-weighted* nature of the coefficients. Close observation indicates also that the solutions for any longitudinal component, whether permanent, induced, or part of a combination, only differ by geometric constants. Consequently, for a model where the coefficients of the solutions are determined by some semi-empirical fitting technique, all of these solutions may be written

$$\Psi^{out} = c\ A\ P_1^0(\xi)\ Q_1^0(\eta) \tag{B100}$$

A similar observation can be made for the y-magnetization solutions, with the solutions all taking the form

$$\Psi^{out} = c\ B\ P_1^1(\xi)\ Q_1^1(\eta)\ \sin\ \phi \tag{B101}$$

and, although the z-magnetization solutions were not generated specifically, they can be formed from any of the y-magnetization solutions by simple interchange of y and z, and written as

$$\Psi^{out} = c\ C\ P_1^1(\xi)\ Q_1^1(\eta)\ \cos\ \phi \tag{B102}$$

This common form for the equations, implies that whatever the nature of the magnetization of the vessel, whether permanent, induced, or mixed, the model need only use the three equations (B100)-(B102).

To obtain the external magnetic field and induction from these solutions, we use the Cartesian co-ordinate form for $\vec{\nabla}\Psi^{out}$ given in (B32) together with the derivatives (B33)-(B35). Tedious rearrangement, leads to the field components presented earlier in Section 5.1.

B.5.1 ASYMPTOTIC LIMITS

It is worth pointing out that as $a \rightarrow 0$ and $b \rightarrow 0$ and the spheroid shrinks to a point, the asymptotic expansions of (B92)-(B99) are, as might be expected, equal to the point dipole equations. Furthermore, as $a \rightarrow b$ and the spheroid becomes spherical, the two demagnetizing factors N_L and N_T tend to the familiar value of $1/3$.

C POSITION OPTIMIZATION DERIVATIVES

To evaluate the derivatives

$$D_{ij} = \frac{\partial \epsilon_i}{\partial p_j} = \frac{\partial}{\partial p_j} \underset{\sim i \sim}{R^T w} = \frac{\partial}{\partial p_j} \sum_k \left(\underset{\sim i}{R^T}(p) \underset{\sim}{} \right)_k (\underset{\sim}{w})_k \delta_{\beta_1 \beta_2} \quad \text{where} \quad i \subset \alpha,\ j \subset \beta_1,\ k \subset \beta_2 \quad \text{(C103)}$$

required for the position-optimization process of Section 8, we need to calculate

$$\left(\frac{\partial}{\partial x_\beta}, \frac{\partial}{\partial y_\beta}, \frac{\partial}{\partial z_\beta}, \frac{\partial}{\partial c_\beta}\right) \underset{\approx}{h}^{(\alpha\beta)} = \left(\frac{\partial}{\partial x_\beta}, \frac{\partial}{\partial y_\beta}, \frac{\partial}{\partial z_\beta}, \frac{\partial}{\partial c_\beta}\right) \underset{\approx}{h} (\vec{r}_\alpha - \vec{r}_\beta, c_\beta)$$

$$= -\left(\frac{\partial}{\partial x}, \frac{\partial}{\partial y}, \frac{\partial}{\partial z}, -\frac{\partial}{\partial c}\right) \underset{\approx}{h} (\vec{r}, c)\Big|_{\vec{r}=\vec{r}_\alpha - \vec{r}_\beta,\ c=c_\beta} \quad \text{(C104)}$$

where α corresponds to a measurement point and β to the location of a source site. The derivatives can be evaluated from expressions such as

$$\partial \underset{\approx}{h} / \partial \zeta = \partial \xi / \partial \zeta \ \partial \underset{\approx}{h} / \partial \xi \ + \ \partial \eta / \partial \zeta \ \partial \underset{\approx}{h} / \partial \eta \ + \ \partial \phi / \partial \zeta \ \partial \underset{\approx}{h} / \partial \phi \quad \text{(C105)}$$

where ζ is one of $\{x, y, z, c\}$, together with the derivatives (B33)-(B35).

After some tedious manipulation, we arrive at the following elements which must all be multiplied by $c^{-1} \left(\eta^2 - \xi^2\right)^{-3}$ and then subjected to the appropriate sign changes of (C104).

Components of $\partial \underset{\approx}{h} / \partial x$

$\partial hxx / \partial x =$

$$\xi \left(3\eta^2 - 5\xi^2\eta^2 + \xi^4 + \xi^2\right) \quad \text{(C106)}$$

$\partial hxy / \partial x =$

$$\frac{2 \sin(\phi) \eta \sqrt{1-\xi^2} \left(3\xi^2 - 5\xi^2\eta^2 + \xi^4 + \eta^2\right)}{\sqrt{\eta^2 - 1}} \quad \text{(C107)}$$

$\partial hxz / \partial x =$

$$\frac{2 \cos(\phi) \eta \sqrt{1-\xi^2} \left(3\xi^2 - 5\xi^2\eta^2 + \xi^4 + \eta^2\right)}{\sqrt{\eta^2 - 1}} \quad \text{(C108)}$$

$\partial hyx/\partial x =$

$$\frac{\sin(\phi)\eta\sqrt{1-\xi^2}\,(3\,\xi^2-5\,\xi^2\eta^2+\xi^4+\eta^2)}{\sqrt{\eta^2-1}} \tag{C109}$$

$\partial hyy/\partial x =$

$$\frac{2\,\xi\,(5\,\eta^4\xi^2-4\,\eta^4-\xi^4\eta^2-4\,\xi^2\eta^2+\xi^2+3\,\eta^2)}{\eta^2-1} -$$

$$\frac{2\,\xi\,(\xi^2-1)\,(-\xi^2\eta^2-\xi^2-3\,\eta^2+5\,\eta^4)\cos(\phi)^2}{\eta^2-1} \tag{C110}$$

$\partial hyz/\partial x =$

$$\frac{\xi\sin(2\,\phi)\,(\xi^2-1)\,(-\xi^2\eta^2-\xi^2-3\,\eta^2+5\,\eta^4)}{\eta^2-1} \tag{C111}$$

$\partial hzx/\partial x =$

$$\frac{\cos(\phi)\eta\sqrt{1-\xi^2}\,(3\,\xi^2-5\,\xi^2\eta^2+\xi^4+\eta^2)}{\sqrt{\eta^2-1}} \tag{C112}$$

$\partial hzy/\partial x =$

$$\frac{\xi\sin(2\,\phi)\,(\xi^2-1)\,(-\xi^2\eta^2-\xi^2-3\,\eta^2+5\,\eta^4)}{\eta^2-1} \tag{C113}$$

$\partial hzz/\partial x =$

$$\frac{2\,\xi\,(\xi^2-1)\,(-\xi^2\eta^2-\xi^2-3\,\eta^2+5\,\eta^4)\cos(\phi)^2}{\eta^2-1}+\frac{2\,\xi\,(\eta^2-\xi^2)^2}{\eta^2-1} \tag{C114}$$

Components of $\partial \underset{\sim}{h}/\partial y$

$\partial hxx/\partial y =$

$$\frac{\sin(\phi)\eta\sqrt{1-\xi^2}\,(3\,\xi^2-5\,\xi^2\eta^2+\xi^4+\eta^2)}{\sqrt{\eta^2-1}} \tag{C115}$$

$$\partial hxy/\partial y =$$

$$\frac{2\,\xi\,\left(5\,\eta^4\xi^2 - 4\,\eta^4 - \xi^4\eta^2 - 4\,\xi^2\eta^2 + \xi^2 + 3\,\eta^2\right)}{\eta^2 - 1}$$

$$-\frac{2\,\xi\,\left(\xi^2 - 1\right)\left(-\xi^2\eta^2 - \xi^2 - 3\,\eta^2 + 5\,\eta^4\right)\cos(\phi)^2}{\eta^2 - 1} \tag{C116}$$

$$\partial hxz/\partial y =$$

$$\frac{\xi\,\sin(2\,\phi)\,\left(\xi^2 - 1\right)\left(-\xi^2\eta^2 - \xi^2 - 3\,\eta^2 + 5\,\eta^4\right)}{\eta^2 - 1} \tag{C117}$$

$$\partial hyx/\partial y =$$

$$\frac{\xi\,\left(5\,\eta^4\xi^2 - 4\,\eta^4 - \xi^4\eta^2 - 4\,\xi^2\eta^2 + \xi^2 + 3\,\eta^2\right)}{\eta^2 - 1}$$

$$-\frac{\xi\,\left(\xi^2 - 1\right)\left(-\xi^2\eta^2 - \xi^2 - 3\,\eta^2 + 5\,\eta^4\right)\cos(\phi)^2}{\eta^2 - 1} \tag{C118}$$

$$\partial hyy/\partial y =$$

$$\left(\frac{2\,\eta\,\left(1 - \xi^2\right)^{3/2}\left(-3\,\xi^2 - \xi^2\eta^2 + 5\,\eta^4 - \eta^2\right)\cos(\phi)^2}{\left(\eta^2 - 1\right)^{3/2}}\right.$$

$$\left.+\frac{2\,\eta\,\sqrt{1 - \xi^2}\,\left(5\,\eta^4\xi^2 - \xi^4\eta^2 + 3\,\xi^2 - 6\,\xi^2\eta^2 - 2\,\eta^4 + \eta^2\right)}{\left(\eta^2 - 1\right)^{3/2}}\right)\sin(\phi) \tag{C119}$$

$$\partial hyz/\partial y =$$

$$\frac{2\,\eta\,\left(1 - \xi^2\right)^{3/2}\left(-3\,\xi^2 - \xi^2\eta^2 + 5\,\eta^4 - \eta^2\right)\cos(\phi)^3}{\left(\eta^2 - 1\right)^{3/2}}$$

$$+\frac{2\,\eta\,\sqrt{1 - \xi^2}\,\left(-4\,\eta^4 - \xi^4\eta^2 + 5\,\eta^4\xi^2 + \eta^2 - 2\,\xi^2\eta^2 - 2\,\xi^4 + 3\,\xi^2\right)\cos(\phi)}{\left(\eta^2 - 1\right)^{3/2}} \tag{C120}$$

$\partial hzx/\partial y =$

$$\frac{\xi \sin(2\phi)\left(\xi^2-1\right)\left(-\xi^2\eta^2-\xi^2-3\eta^2+5\eta^4\right)}{2\eta^2-2} \tag{C121}$$

$\partial hzy/\partial y =$

$$\frac{2\eta\left(1-\xi^2\right)^{3/2}\left(-3\xi^2-\xi^2\eta^2+5\eta^4-\eta^2\right)\cos(\phi)^3}{\left(\eta^2-1\right)^{3/2}}$$

$$+\frac{2\eta\sqrt{1-\xi^2}\left(-4\eta^4-\xi^4\eta^2+5\eta^4\xi^2+\eta^2-2\xi^2\eta^2-2\xi^4+3\xi^2\right)\cos(\phi)}{\left(\eta^2-1\right)^{3/2}} \tag{C122}$$

$\partial hxz/\partial y =$

$$-\left(\frac{2\eta\left(1-\xi^2\right)^{3/2}\left(-3\xi^2-\xi^2\eta^2+5\eta^4-\eta^2\right)\cos(\phi)^2}{\left(\eta^2-1\right)^{3/2}}\right.$$

$$\left.-\frac{2\eta\sqrt{1-\xi^2}\left(\eta^2-\xi^2\right)^2}{\left(\eta^2-1\right)^{3/2}}\right)\sin(\phi) \tag{C123}$$

Components of $\partial \underset{\approx}{h}/\partial z$

$\partial hxx/\partial z =$

$$\frac{\cos(\phi)\eta\sqrt{1-\xi^2}\left(3\xi^2-5\xi^2\eta^2+\xi^4+\eta^2\right)}{\sqrt{\eta^2-1}} \tag{C124}$$

$\partial hxy/\partial z =$

$$\frac{\xi \sin(2\phi)\left(\xi^2-1\right)\left(-\xi^2\eta^2-\xi^2-3\eta^2+5\eta^4\right)}{\eta^2-1} \tag{C125}$$

$\partial hxx/\partial z =$

$$\frac{2\xi\left(\xi^2-1\right)\left(-\xi^2\eta^2-\xi^2-3\eta^2+5\eta^4\right)\cos(\phi)^2}{\eta^2-1}+\frac{2\xi\left(\eta^2-\xi^2\right)^2}{\eta^2-1} \tag{C126}$$

$\partial hyx/\partial z =$

$$\frac{\xi \sin(2\phi)\left(\xi^2-1\right)\left(-\xi^2\eta^2-\xi^2-3\eta^2+5\eta^4\right)}{2\eta^2-2} \tag{C127}$$

$\partial hyy/\partial z =$

$$\frac{2\eta\left(1-\xi^2\right)^{3/2}\left(-3\xi^2-\xi^2\eta^2+5\eta^4-\eta^2\right)\cos(\phi)^3}{\left(\eta^2-1\right)^{3/2}}$$

$$+\frac{2\eta\sqrt{1-\xi^2}\left(-4\eta^4-\xi^4\eta^2+5\eta^4\xi^2+\eta^2-2\xi^2\eta^2-2\xi^4+3\xi^2\right)\cos(\phi)}{\left(\eta^2-1\right)^{3/2}} \tag{C128}$$

$\partial hyz/\partial z =$

$$-\left(\frac{2\eta\left(1-\xi^2\right)^{3/2}\left(-3\xi^2-\xi^2\eta^2+5\eta^4-\eta^2\right)\cos(\phi)^2}{\left(\eta^2-1\right)^{3/2}}-\frac{2\eta\sqrt{1-\xi^2}\left(\eta^2-\xi^2\right)^2}{\left(\eta^2-1\right)^{3/2}}\right)\sin(\phi) \tag{C129}$$

$\partial hzx/\partial z =$

$$\frac{\xi\left(\xi^2-1\right)\left(-\xi^2\eta^2-\xi^2-3\eta^2+5\eta^4\right)\cos(\phi)^2}{\eta^2-1}+\frac{\xi\left(\eta^2-\xi^2\right)^2}{\eta^2-1} \tag{C130}$$

$\partial hzy/\partial z =$

$$\left(\frac{2\eta\left(1-\xi^2\right)^{3/2}\left(-3\xi^2-\xi^2\eta^2+5\eta^4-\eta^2\right)\cos(\phi)^2}{\left(\eta^2-1\right)^{3/2}}-\frac{2\eta\sqrt{1-\xi^2}\left(\eta^2-\xi^2\right)^2}{\left(\eta^2-1\right)^{3/2}}\right)\sin(\phi) \tag{C131}$$

$\partial hzz/\partial z =$

$$-\frac{2\eta\left(1-\xi^2\right)^{3/2}\left(-3\xi^2-\xi^2\eta^2+5\eta^4-\eta^2\right)\cos(\phi)^3}{\left(\eta^2-1\right)^{3/2}}+\frac{6\eta\sqrt{1-\xi^2}\left(\eta^2-\xi^2\right)^2\cos(\phi)}{\left(\eta^2-1\right)^{3/2}} \tag{C132}$$

Components of $\partial \underset{\approx}{h}/\partial c$

$\partial hxx/\partial c =$

$$\eta\left(3\xi^2\eta^2-\eta^2+\xi^4-3\xi^2\right) \tag{C133}$$

$\partial hxy/\partial c =$

$$2\,\xi\,\sqrt{\eta^2-1}\sqrt{1-\xi^2}\left(\xi^2+3\,\eta^2\right)\sin(\phi) \tag{C134}$$

$\partial hxz/\partial c =$

$$2\,\xi\,\sqrt{\eta^2-1}\sqrt{1-\xi^2}\left(\xi^2+3\,\eta^2\right)\cos(\phi) \tag{C135}$$

$\partial hyx/\partial c =$

$$\xi\,\sqrt{\eta^2-1}\sqrt{1-\xi^2}\left(\xi^2+3\,\eta^2\right)\sin(\phi) \tag{C136}$$

$\partial hyy/\partial c =$

$$\frac{2\,\eta\,\left(\xi^2-1\right)\left(\xi^2\eta^2-3\,\xi^2+3\,\eta^4-\eta^2\right)\cos(\phi)^2}{\eta^2-1}$$

$$-\frac{2\,\eta\,\left(3\,\eta^4\xi^2-2\,\eta^4+\eta^2-2\,\xi^4-4\,\xi^2\eta^2+\xi^4\eta^2+3\,\xi^2\right)}{\eta^2-1} \tag{C137}$$

$\partial hyz/\partial c =$

$$-\frac{\eta\,\sin(2\,\phi)\left(\xi^2-1\right)\left(\xi^2\eta^2-3\,\xi^2+3\,\eta^4-\eta^2\right)}{\eta^2-1} \tag{C138}$$

$\partial hzx/\partial c =$

$$\xi\,\sqrt{\eta^2-1}\sqrt{1-\xi^2}\left(\xi^2+3\,\eta^2\right)\cos(\phi) \tag{C139}$$

$\partial hzy/\partial c =$

$$-\frac{\eta\,\sin(2\,\phi)\left(\xi^2-1\right)\left(\xi^2\eta^2-3\,\xi^2+3\,\eta^4-\eta^2\right)}{\eta^2-1} \tag{C140}$$

$\partial hzz/\partial c =$

$$-\frac{2\,\eta\,\left(\xi^2-1\right)\left(\xi^2\eta^2-3\,\xi^2+3\,\eta^4-\eta^2\right)\cos(\phi)^2}{\eta^2-1}-\frac{2\,\eta\,\left(\eta^2-\xi^2\right)^2}{\eta^2-1} \tag{C141}$$

References

[1] G.-M Yan, X.-T. Weng, Yuan Fang, X.-C. Zhang, and G.-L. Sun. The mathematical model of the magnetic field of a vessel - an array of uniformly magnetized spheroids. In *Mine Warfare Vessels and Systems 2 - Vol II*, 10 Upper Belgrave Sq., London, SW1X 8BQ., May 1989. The Royal Institute of Naval Architects.

[2] I. Barrodale, C.A. Zala, and N.R. Chapman. Comparison of the ℓ_1 and ℓ_2 norms applied to one-at-a-time spike extraction from seismic traces. *Geophysics*, 49(11):2048–52, Nov 1984.

[3] G.H. Golub and C.F. Van Loan. *Matrix Computations*. John Hopkins University Press (Baltimore), 2nd edition, 1989.

[4] J.H. Wilkinson and C. Reinsch. *Linear Algebra*. Springer-Verlag (New York), 1971.

[5] R.A. Horn and C.R. Johnson. *Matrix Analysis*. Cambridge University Press, 1990.

[6] S. Perlis. *Theory of Matrices*. Addison-Wesley (Cambridge, Mass), 1952.

[7] D. McKirdy. Second derivative approach to least squares estimation. Unpublished DREP Contractor's Report, 1990.

[8] P.M. Morse and H. Feshbach. *Methods of Theoretical Physics*. McGraw-Hill (New York), 1953.

DISTRIBUTION

REPORT NO.: DREP Report 93-81

TITLE: NEW APPROACHES TO MAGNETIC MODELLING
I. PROLATE SPHEROIDS
II. ONE-SPIKE-AT-A-TIME FITTING

AUTHOR: P. M. Holtham and C. E. Lucas

DATED: November 1993

SECURITY GRADING: UNCLASSIFIED

DISTRIBUTION LIST

18 - DREP
- 14 - Library
- 1 - Dr. P.M. Holtham
- 1 - Dr. R.H. Kuwahara
- 1 - Mr. R.E. Erickson
- 1 - Circulate Dr. H.S. Wilson, Mr. T.C. Richards, Mr. J.B. Nelson

1 - NEUA - CSEO/Mr. I. Cobb
1 - NEUP - MS/Mr. G. Morin

3 - NDHQ
- 1 - CRAD
- 1 - DMCS - Mr. E Wessman
- 1 - DNR

2 - DSIS
2 - DREA
2 - Barrodale Computing Services

UNITED STATES
- 1 - NSWC - Mr. M. Gresco
- 1 - NSWC - Dr. J. Holmes
- 1 - NSWC - Mr. P. Winters
- 1 - NSWC - Mr. I. Smith

UK
1 - DRA - Mr. A. Dudley
1 - DRA - Dr. A.W. Moore
1 - DRA - Mr. G. Field

AUSTRALIA
1 - DSTO - Mr. Kevin Gaylor
1 - DSTO - Dr. Alan Theobald

NEW ZEALAND
1 - DSE - Mr. I. Rumball

Unclassified

SECURITY CLASSIFICATION OF FORM
(highest classification of Title, Abstract, Keywords)

DOCUMENT CONTROL DATA

(Security classification of title, body of abstract and indexing annotation must be entered when the overall document is classified)

1. ORIGINATOR (the name and address of the organization preparing the document. Organizations for whom the document was prepared, e.g. Establishment sponsoring a contractor's report, or tasking agency, are entered in section 8.)

Defence Research Establishment Pacific

2. SECURITY CLASSIFICATION (overall security classification of the document including special warning terms if applicable)

UNCLAS

3. TITLE (the complete document title as indicated on the title page. Its classification should be indicated by the appropriate abbreviation (S,C or U) in parentheses after the title.)

New Approaches to Magnetic Modelling
I Prolate Spheroids
II One-Spike-At-A-Time Fitting

4. AUTHORS (Last name, first name, middle initial)

HOLTHAM, Peter M. and LUCAS, Carmen E.

5. DATE OF PUBLICATION (month and year of publication of document)

Nov 93

6a. NO. OF PAGES (total containing information. Include Annexes, Appendices, etc.)

65

6b. NO. OF REFS (total cited document)

8

7. DESCRIPTIVE NOTES (the category of the document, e.g. technical report, technical note or memorandum. If appropriate, enter the type report, e.g. interim, progress, summary, annual or final. Give the inclusive dates when a specific reporting period is covered.)

DREP Report 93-81

8. SPONSORING ACTIVITY (the name of the department project office or laboratory sponsoring the research and development. Include the address.)

9a. PROJECT OR GRANT NO. (if appropriate, the applicable research and development project or grant number under which the document was written. Please specify whether project or grant)

9b. CONTRACT NO. (if appropriate, the applicable number under which the document was written)

10a. ORIGINATOR'S DOCUMENT NUMBER (the official document number by which the document is identified by the originating activity. This number must be unique to this document.)

DREP Report 93-81

10b. OTHER DOCUMENT NOS. (Any other numbers which may be assigned this document either by the originator or by the sponsor)

11. DOCUMENT AVAILABILITY (any limitations on further dissemination of the document, other than those imposed by security classificati

(X) Unlimited distribution
( ) Distribution limited to defence departments and defence contractors; further distribution only as approved
( ) Distribution limited to defence departments and Canadian defence contractors; further distribution only as approved
( ) Distribution limited to government departments and agencies; further distribution only as approved
( ) Distribution limited to defence departments; further distribution only as approved
( ) Other (please specify):

12. DOCUMENT ANNOUNCEMENT (any limitation to the bibliographic announcement of this document. This will normally correspond to the Document Availability (11). However, where further distribution (beyond the audience specified in 11) is possible, a wider announcement audience may be selected.)

Unclassified

Unclassified

SECURITY CLASSIFICATION OF FORM

13. ABSTRACT (a brief and factual summary of the document. It may also appear elsewhere in the body of the document itself. It is highly desirable that the abstract of classified documents be unclassified. Each paragraph of the abstract shall begin with an indication of the security classification of the information in the paragraph (unless the document itself is unclassified) represented as (S), (C), or (U). It is not necessary to include here abstracts in both offical languages unless the text is bilingual).

As article

14. KEYWORDS, DESCRIPTORS or IDENTIFIERS (technically meaningful terms or short phrases that characterize a document and could be helpful in cataloguing the document. They should be selected so that no security classification is required. Identifiers, such as equipment model designation, trade name, military project code name, geographic location may also be included. If possible keywords should be selected from a published thesaurus, e.g. Thesaurus of Engineering and Scientific Terms (TEST) and that thesaurus-identified. If it is not possible to select indexing terms which are Unclassified, the classification of each should be indicated as with the title.)

√ Magnetic modelling
Prolate spheroid modelling
√ Ship signatures
√ Magnetic signatures
√ Mine simulation
√ least-squares filling